RSC Advances

REVIEW

View Article Online
View Journal | View Issue

Cite this: *RSC Adv.*, 2025, **15**, 34340

Three decades of selective product formation *via* Griesbaum co-ozonolysis: insight and advances (1995–2025)

Muhammad Zain-ul-Abideen,[a] Aamer Saeed, *[a] Mian Bilal Haider,[a] Ghulam Shabir[a] and Hesham R. El-Seedi[b]

Received 2nd August 2025
Accepted 1st September 2025

DOI: 10.1039/d5ra05620a

rsc.li/rsc-advances

The Griesbaum co-ozonolysis reaction was first described by Karl Griesbaum and his collaborators in the mid-1990s. Their pioneering work laid the foundation for synthesis of tetrasubstituted ozonides by the reaction of *O*-methyl oximes with carbonyl compounds in the presence of ozone. It has emerged as a powerful and selective alternative to conventional ozonolysis. This review highlights the unique advantages of the reaction, including its high selectivity, operational simplicity, mild conditions, and consistently good yields. Emphasis is placed on the distinctive features that make Griesbaum co-ozonolysis a preferred approach for constructing complex molecular frameworks, *i.e.*, di-, tri- and tetrasubstituted ozonides, mainly spiro and dispiro-1,2,4-trioxolanes, triterpenoids and synthetic drug candidates. The reaction tolerates basic conditions, allowing for controlled functionalization, and has been applied in post-ozonolysis transformation and chemical sensor development. Importantly, it eliminates the need for tetrasubstituted alkenes, broadening accessibility to complex ozonides. A comprehensive survey of the literature from the past three decades is presented, focusing on the diverse range of products synthesized using this method. The review underscores the growing importance and synthetic utility of Griesbaum co-ozonolysis in modern synthetic, organic and medicinal chemistry.

1. Introduction

The direct ozonolysis of tetrasubstituted olefins seldom affords the corresponding tetrasubstituted ozonides. The challenge arises for several reasons: first, the synthesis of suitably substituted olefins is itself nontrivial as steric hindrance around the double bond often hinders their preparation. Second, even when accessible, tetrasubstituted olefins display reduced reactivity toward ozone due to steric shielding of the π-bond. Third, ozonolysis of hindered olefins frequently leads to an unstable or short-lived carbonyl oxide intermediate, which undergoes decomposition, side reactions, or rearrangement, rather than productive cycloaddition to stable ozonides. These combined limitations indicate that direct ozonolysis rarely furnishes isolable tetrasubstituted ozonides in useful yields. This fact provides a major impetus for the development of Griesbaum co-ozonolysis, which bypasses the need for tetrasubstituted olefins altogether.

Described by K. Griesbaum and colleagues in 1995, Griesbaum co-ozonolysis is an attractive conversion in organic chemistry that enables the formation of tetrasubstituted ozonides (particularly 1,2,4-trioxolanes) with enhanced stability compared to conventional ozonolysis products. The reaction employs *O*-methyl oximes and carbonyl compounds as substrates, using ozone as the oxidizing agent, to produce 1,2,4-trioxolanes (Fig. 1).

An *O*-methyl oxime reacts with ozone to form a carbonyl oxide, which is proposed to undergo 1,3-dipolar cycloaddition with a ketone to form a cyclic stable ozonide. One mechanistic hypothesis suggests that the reaction may proceed *via* a pathway analogous to the Story–Murray–Youssefyen mechanism,[1] rather than exclusively through the conventional carbonyl oxide pathway. In this proposal, the carbonyl compound **2** is inserted into the peroxide bond of intermediate **5**, leading to the formation of adduct **6**. This intermediate can then eliminate methyl nitrite, resulting in the formation of ozonide **3**, as illustrated by the electron flow arrows in structure **6**. Although this route has been reported to occur only to a negligible extent in the ozonolysis of olefin,[2] it may be operative under specific conditions, such as during the ozonolysis of *ortho*-methyl oximes (Fig. 2). Nevertheless, the precise mechanism of Griesbaum co-ozonolysis remains not fully understood, and further studies are required to clarify the operative pathways.

In 1995, K. Griesbaum *et al.*[3,4] reported a distinctive type of ozonolysis that has since become known as Griesbaum co-ozonolysis. This process involves the ozonolysis of *ortho*-methyl oximes in the presence of substituted acyclic or cyclic

[a]*Department of Chemistry, Quaid-i-Azam University, Islamabad 45320, Pakistan. E-mail: asaeed@qau.edu.pk; Fax: +92-51-9064-2241; Tel: +92-51-9064-2128*
[b]*Department of Chemistry, Faculty of Science, Islamic University of Madinah, Madinah, 42351, Saudi Arabia*

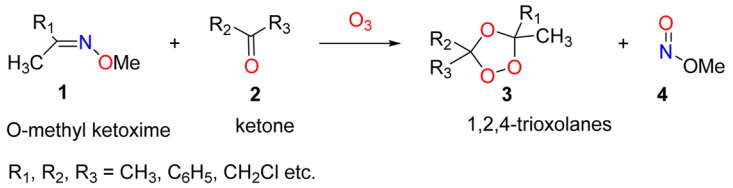

Fig. 1 General scheme of the Griesbaum co-ozonolysis reaction.

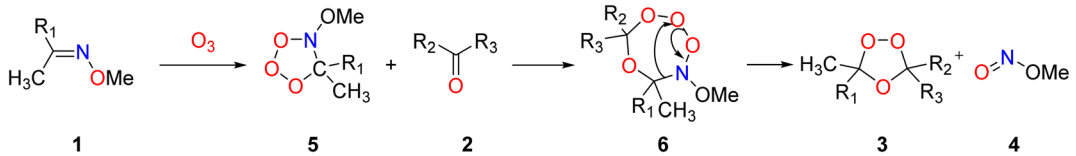

Fig. 2 Mechanism of the Griesbaum co-ozonolysis reaction.

carbonyl compounds to selectively form ozonides. Compared to conventional olefin ozonolysis, this method offers several significant advantages, as follows. With the elimination of the need for olefin precursors, it bypasses the synthesis of parent olefin entirely. With improved selectivity, the preparation of unsymmetrically substituted ozonides proceeds without the formation of undesired byproduct ozonides, which are typically encountered in the ozonolysis of unsymmetrical olefins. With the dual synthetic pathway (routes A and B), this flexibility enables optimization of the ozonide yields by selecting a pair of substrates wherein the more reactive carbonyl compound drives the reaction efficiently.[5] With the access to otherwise unattainable ozonides, in certain cases, this co-ozonolysis method is the only viable route to obtain specific ozonides. For example, the ozonide of tetramethylethylene (**3**) could not be synthesized *via* conventional olefin ozonolysis in solution, but was successfully obtained through this approach (Fig. 2).

Three distinct classes of reactants have been identified in Griesbaum co-ozonolysis, based on the structural nature and branching of the starting materials. The type I reaction involves both *O*-methyl ketoximes and substituted ketones **2** that are acyclic in nature (Fig. 2). The type II reaction utilizes cyclic ketoximes **7** in combination with acyclic ketones **10** (Fig. 3). The type III reaction involves the use of cyclic ketoximes **7** with cyclic ketones **9** of varying ring sizes, leading to formation of ozonide products **12** and **11**, respectively (Fig. 3).

A key intermediate 6 is generated during the Griesbaum co-ozonolysis process, which is not observed in conventional olefin ozonolysis. This mechanistic distinction accounts for the structural difference between the product obtained *via* Griesbaum co-ozonolysis and those formed from standard olefin ozonolysis. This unique feature underscores the synthetic utility of the reaction. In particular, this methodology applied to the synthesis of spirocyclic trioxolanes *via* the reaction of cyclic ketones with *O*-methyl oximes, where the newly generated spiro-center can lead to four possible diastereomers.

These stereoisomers can be selectively obtained under stereo selectivity or regioselective reaction conditions.

2. *N*-Methoxy-1,2,4-dioxazolidines *via* ozonolysis reaction

Griesbaum *et al.*[6] reported the formation of dioxazolidines as a continuation of his previous work. The synthesis carried out by the ozonolysis of ethyl vinyl ether in the presence of the *O*-methylated oxime of cyclohexanone resulted in the formation of *N*-methoxy-1,2-dioxa-4-azaspiro[4.5]decane. Additionally, the ozonolysis of *O*-methylated dioximes derived from 1,4- and 1,5-

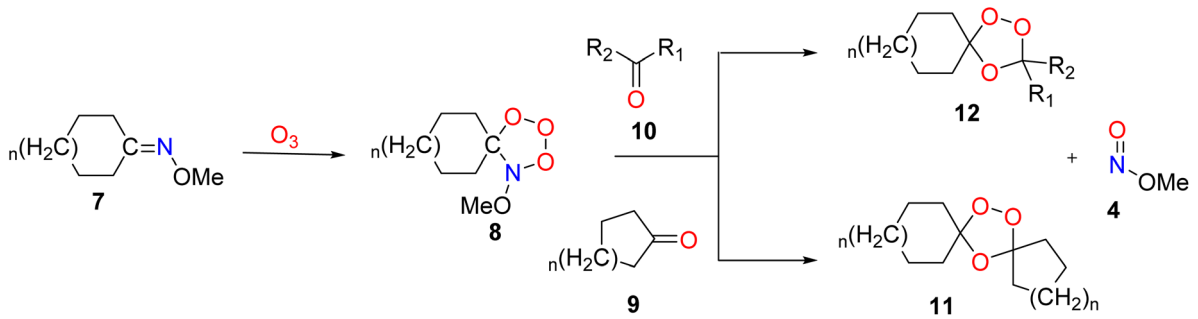

Fig. 3 Cyclic *O*-methyl ketoxime treated with cyclic and acyclic ketones.

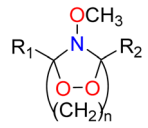

13

R_1=R_2= CH3, n= 3

50%

Fig. 4 *N*-Methoxylated bicyclic-1,2,4-dioxazolidines **13**.

dicarbonyl compounds afforded *N*-methoxylated bicyclic 1,2,4-dioxazolidines **13**.

This study extends the established concept of carbonyl oxide–imine cycloaddition commonly used to generate 2,3-dioxazolidines to include the reaction involving unsubstituted carbonyl oxide and *O*-methylated oxime, forming *N*-methoxy-substituted dioxazolidine. Notably, substituted carbonyl oxide did not undergo this transformation. The absence of such products in the ozonolysis reaction of *O*-methylated oximes with ketones, unlike the reaction with alkyl or aryl imines, suggests that *O*-methylated oximes are significantly less dipolarophilic compared to ketones. Importantly, this work represents the first report of a one-step synthesis for bicyclic *N*-methoxy-substituted 1,2,4-dioxazolidines, with compounds **13** offering the highest isolated yield. These findings introduce the known examples of these unique heterocyclic scaffolds (Fig. 4).

3. Post-ozonolysis transformations

With these ozonides in hand, attention was then directed to their post-ozonolysis functionalization. Although the Griesbaum co-ozonolysis is a powerful method, the synthetic utility of functionalized tetra-substituted ozonides remain underexplored.[7,8] Nevertheless, several successful transformations of di-, tri-, and tetra-substituted ozonides have been reported. For example, ozonide ketones and aldehydes[9] have been reduced to their corresponding alcohols using lithium or sodium borohydride. Ozonide alcohol has been oxidized to aldehyde *via* Swern oxidation and ozonide aldehydes converted to dimethyl or 1,3-dioxolane acetals,[10,11] which serve as intermediates for further C–C bond forming reactions. These include allylation with allylzinc bromide allyl silanes or allylstannanes in the presence of $TiCl_4$ or $SnCl_4$ and Mukaiyama-type aldol condensations (Fig. 5).

R-Oxo-ozonides, where the carbonyl is at the *R*-position, can be synthesized *via* Griesbaum co-ozonolysis[12] and further transformed into *O*-methyl oximes or epoxides using *O*-methylhydroxylamine or diazomethane, respectively.[13] *R*-Chloro ozonides undergo substitution with alcohol to afford ozonide ether, either in the presence[14] or absence of $AgBF_4$. *R*-Acetoxy ozonides similarly react to alcohols under $NaHCO_3$-mediated conditions.

Unsaturated ozonides have also been derivatized[15] by bromination of vinyl and vinylidene ozonides to yield dibromo derivatives. Diimide reduction of unsaturated bicyclic ozonides affords saturated analogs.[16] Vinyl chloride ozonide undergoes methanolysis to form methyl ester ozonides, and the stepwise treatment with *m*-CPBA and $AgBF_4$ yields enone ozonides *via* epoxy intermediates.[17]

For post-ozonolysis transformations, reaction temperatures were maintained below 60 °C to prevent ozonide decomposition *via* Hock-type fragmentation into adamantane lactone and parent cyclohexanones (Fig. 6).[18] Notably, these ozonides exhibit excellent stability under basic conditions and mild

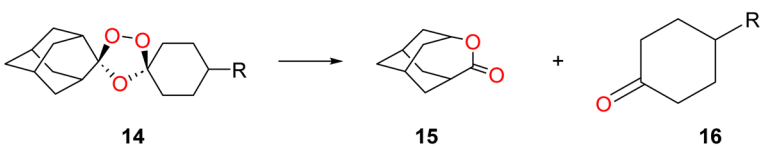

14 15 16

Fig. 5 Decomposition of ozonide.

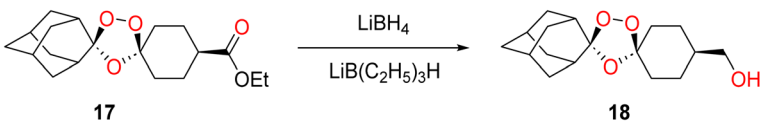

17 18

Fig. 6 Post-ozonolysis reduction of ozonide ester to ozonide alcohol.

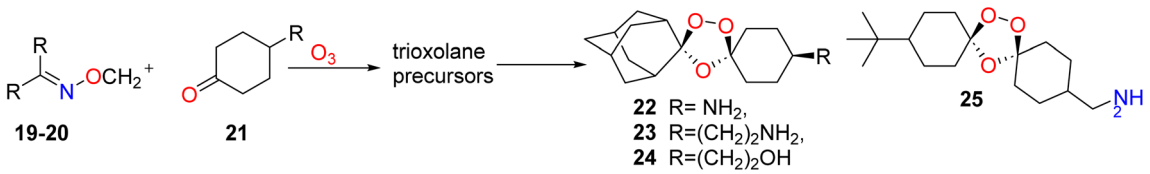

Fig. 7 Synthesis of trioxolane by Griesbaum co-ozonolysis and post-ozonolysis transformation.

acidic treatments, including those for Boc deprotection. Additionally, reductive amination of ozonide aldehyde was feasible, with stability attributed to the absence of alpha hydrogen that otherwise promoted Kornblum–DeLaMare fragmentation.[19]

The diastereoselectivity observed in the Griesbaum co-ozonolysis strongly suggests a preference for axial side attack of the carbonyl oxide,[20] governed primarily by the conformation rigidity of the cyclohexanone scaffold. While the electronic effect from the 4-substituent may contribute, the stereochemical outcomes appear largely controlled by kinetic factors, particularly transition state hyper-conjugation. This study also broadens the scope of ozonide-compatible transformations, including ester to alcohol reductions, reductive aminations, Mitsunobu reactions, nucleophilic substitution with mercaptides and azole anions, addition of organolithium and Grignard reagents, and phthalimide deprotections with hydrazine. While the reactivity of di-, tri-, and tetrasubstituted ozonides under these conditions has yet to be fully defined, the wide scope of post-ozonolysis transformations is reminiscent of those used in the derivatization of semisynthetic artemisinin analogs.[21,22] Trioxolanes **22**, **23**, **24**, and **25** were synthesized *via* post-ozonolysis transformations of their corresponding trioxolane esters and phthalimide derivatives. The precursor ester and phthalimides were obtained through Griesbaum co-ozonolysis,[23] involving *O*-methyl oximes of 2-adamantanone **19** for compounds **22–24**, and 4-*tert*-butyl cyclohexanone **20** for **25** with appropriate 4-substituted cyclohexanones **21** (Fig. 7).[24]

Unexpectedly, in all cases, the major product was methyl-3β,28-di-*O*-acetyl-29,30-bisnorlupan-20-oate (**29**), irrespective of the ketone used. The anticipated ozonolysis product was not detected. This anomalous outcome is attributed to a rearrangement of the secondary ozonide intermediate **28**, involving cleavage of a C–Csp^3 bond and migration of the C_{30} methyl group to the electrophilic oxygen. This transformation is mechanistically analogous to the Baeyer–Villiger type rearrangement of ketones in the presence of peroxides.[26]

A similar rearrangement was previously observed during ozonolysis of a 3-*O*-acetylbetulinic acid ester in EtOAc:MeOH at 70 °C, where the methyl ester of the 29,30-dinor-20-oic acid was isolated in 4% yield as a side product, alongside the expected 29-nor-20-ketone.[27] In contrast, compound **29** was obtained as the major product, an outcome likely influenced by the nature of the substituent on the trioxolane ring. Rearrangements of peroxide ozonolysis products are well documented,[28] particularly among substrates such as allyl alcohols, unsaturated ketones, indoles, and benzofurans.[29]

The secondary ozonides at the C_{20} position of botulin derivatives have been reported to be prone to decomposition. Notably, even the inclusion of a highly electrophilic trifluoromethyl ketone failed to yield the outcome of Griesbaum co-ozonolysis. The structure of **29** comprises six-membered rings A, B, C, and D in *trans*-chair conformations and five-membered ring E adopting a slightly distorted envelope geometry.

4. Anomalous ozonolysis product of 3β,28-di-*O*-acetyl-29-norlupan-20-one-*O*-methyloxime

In 2011,[25] a diacetylbetulin derivative **26** was employed to synthesize 3β,28-di-*O*-acetyl-29-norlupan-20-one-*O*-methyloxime **27** as a precursor to triterpene-1,2,4-trioxolane structures of interest for their potential anti-cancer and anti-malarial activity. Compound **26** was subjected to Griesbaum co-ozonolysis with various ketones (acetone, methyltrifluoro methyl acetone, or cyclohexanone) in a CH_2Cl_2: cyclohexane solvent mixture at 0 °C (Fig. 8).

5. Synthesis of triterpenoid-based trioxolanes and dioxazolidines *via* ozonolysis of allobetulin derivatives

Another promising class of triterpenoid-based peroxide, the 1,2,4-dioxazolidine, was synthesized[30] *via* the Griesbaum method.[31] The *O*-methylated dioxime **32**, derived from the 1,5-dicarbonyl compound of A-secoallobetulin **31**,[32] was ozonized to completion, affording *N*-methoxy-substituted 1,2,4-dioxazolidines **33** and **34** in 55% and 38% yields, respectively, after chromatographic purification (Fig. 9). Notably, the reaction exhibited diastereoselectivity, yielding exclusively the

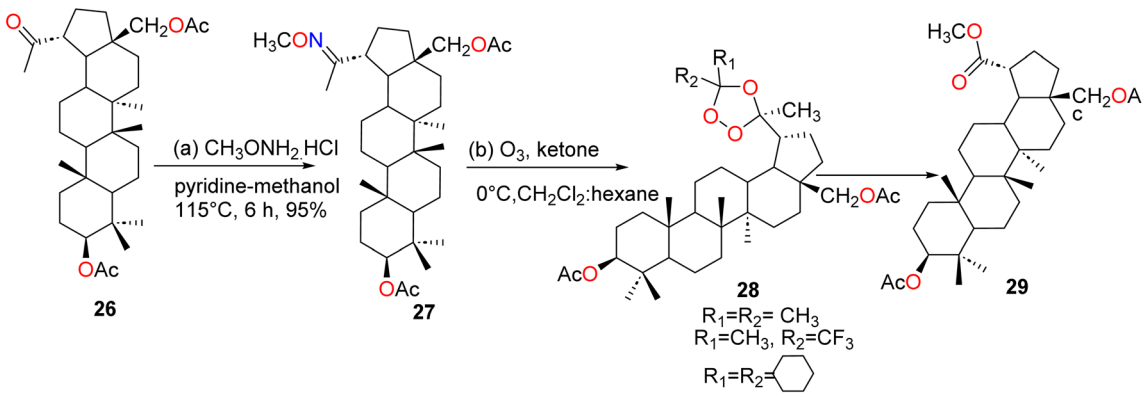

Fig. 8 Synthesis of methyl-3β,28-di-*O*-acetyl-29,30-bisnorlupan-20-oate.

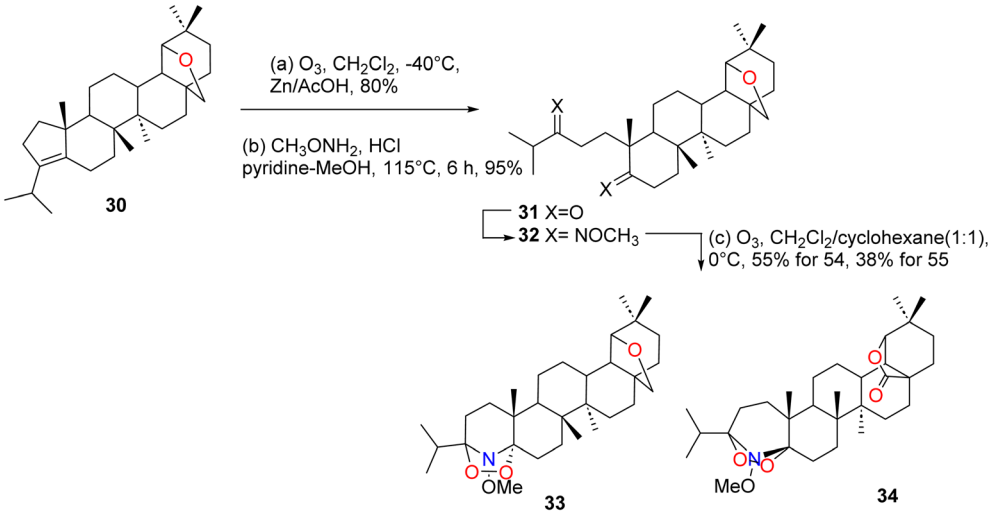

Fig. 9 Synthesis of triterpenoid-based 1,2,4-trioxolanes and 1,2,4-dioxazolidines by ozonolysis of allobetulin derivatives.

(3*S*,5*S*)-configured peroxides as confirmed by X-ray crystallography and the established stereochemistry of allobetulin derivatives. These compounds represent rare examples of stable dioxazolidines, and the first example of *N*-methoxy-1,2,4-dioxazolidines derived from triterpenoids.

6. Stereochemistry of product

The use of symmetrical oxime ether eliminates the possibility of *syn–anti* isomerism in the resulting carbonyl oxide intermediates. This ensures that the stereochemical outcome of the subsequent cycloaddition is determined solely by the geometry of the starting ketones. In the case of achiral benzophenones, the resulting trioxolane products are themselves achiral. For 4-substituted cyclohexanones, the major trioxolane isomers consistently exhibit a *cis*-configuration, wherein the substituent occupies the equatorial position and the peroxo moiety is oriented axially.[33,34] Assuming the stereochemical pathway of the cycloaddition remains consistent across other 4-substituted cyclohexanones, the synthesized trioxolanes were assigned *cis*-configurations.

7. Diastereoselectivity in the Griesbaum co-ozonolysis reaction

The use of a symmetrical oxime ether prevents *syn–anti* isomerism in 2-adamantanone oxide formation, making the stereochemical outcomes dependent solely on the starting cyclohexanone. For 4-substituted cyclohexanones, only two achiral diastereomers *cis* and *trans* are possible (Fig. 10). Co-ozonolysis of compounds **35** and **36** was optimally performed in non-polar solvents at 0 °C, as recommended by Griesbaum.[35,36] For more polar substrates, mixed solvents with minimal dichloromethane content were employed to maintain favorable conditions for ozonide formation. The oxime ether-to-ketone ratio varied between 1.5 : 1 and 1 : 2 to afford **37** and **38** ranging from 20% to 70%, respectively. Product ratios were determined by integration of diagnostic signals in the ^{1}H NMR spectra of crude reaction mixtures. In most cases, only the major isomers **37** were isolated by flash chromatography or crystallization and fully characterized. Stereochemical *cis* or *trans* assignments are based on X-ray crystallography and the assumption of consistent stereochemical outcomes across all cycloaddition products. Stereochemistry assignments cannot be reliably inferred from the chemical shift, coupling constant, or chromatographic behavior. However, X-ray crystallography provides definitive configurations in representative cases. For example, acetoxy ozonide was assigned to a *cis* configuration based on the crystal structure of its hydrolysis product, revealing a chair conformation with the 4-hydroxyphenyl and peroxo groups in equatorial and axial positions, respectively. In group II, X-ray analysis confirmed the major isomer **37** as *cis* and the minor **38** as *trans*, with both the 4-phthalimidomethyl and peroxo groups equatorial in **37**. Collectively, these findings support the conclusion that major cycloaddition products consistently adopt the *cis* configuration 4-substituted cyclohexanones.

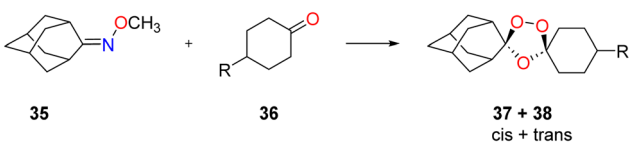

Fig. 10 Diastereoselectivity of Griesbaum co-ozonolysis.

The results demonstrate that diastereoselectivity is influenced by the size and nature of the 4-substituent of the cyclohexanone dipolarophiles. Bulky substituents, such as *tert*-butyl, phenyl, and phthalimido, yielded exclusively one diastereomer, with *cis*/*trans* ratios exceeding 20 : 1. Substrates bearing functional groups linked *via* a single methylene unit exhibited moderate selectivity, with *cis*/*trans* ratios around 5 : 1, suggesting minimal influence from distal substituents. Cyclohexanone substituents with an ester or amide group at the 4-position gave *cis*/*trans* ratios ranging from 2.5 : 1 to 5 : 1.

8. Stereochemistry confirmation *via* analogue synthesis

Due to extensive overlap of the aliphatic signals in the ^{1}H NMR spectra of analogues, unambiguous stereochemical assignment proved difficult. To resolve this, several analogues were synthesized with the aim of obtaining diffraction-quality crystals. Finally, a single crystal of the 4-nitrobenzoate analogue was successfully grown *via* vapor diffusion of hexane into a saturated toluene/ethanol/methanol solution. High-resolution X-ray crystallographic analysis confirmed the anticipated stereochemistry: an axial orientation of the peroxide bridge and a *trans* relationship to the equatorially positioned 3-substituent.

9. Diastereoselective synthesis of triterpenoid trioxolanes *via* Griesbaum co-ozonolysis

Three principal strategies are commonly employed for the synthesis of ozonides in organic chemistry: (i) low-temperature ozonolysis of olefins in aprotic solvents,[37] (ii) co-ozonolysis of *O*-methyl oximes and carbonyl compounds,[38] and (iii) ozone-free methods involving the reaction of 1,5-dicarbonyl compounds and hydrogen peroxide.[39] Among these, the Griesbaum co-ozonolysis method[5] is the most widely adopted, offering high efficiency and structural tenability in the synthesis of peroxide. Using this approach, Vennerstrom[40] synthesized over 200 spiro-1,2,4-trioxolanes incorporating adamantanone scaffolds, which were evaluated for anti-malarial, anti-tumor, and anti-

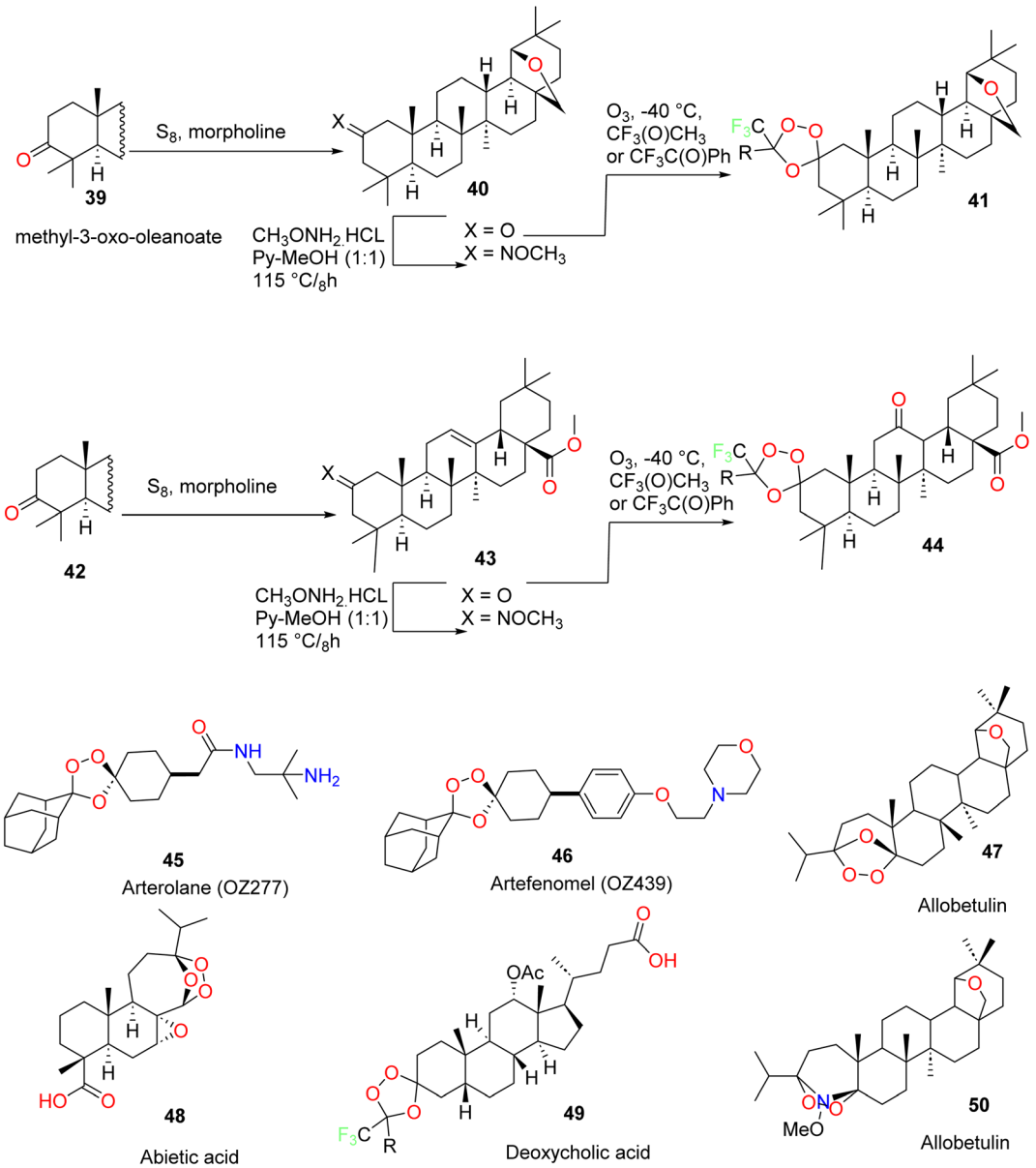

Fig. 11 Peroxides example and synthesis of the CF_3-methylated 1,2,4-trioxolanes derived from oleanane-type triterpenoids.

schistosomal activities. The most promising candidates included OZ277 (Fig. 11), but exhibited potent antimalarial efficacy. As part of ongoing efforts to expand the diversity of biologically active peroxides, the present work[41] describes the synthesis of CF_3-methylated 1,2,4-trioxolanes derived from oleanane-type triterpenoids.

10. Identification of synthetic trioxolane candidate drug development

As reported in ref. 42, in comparison to semi-synthetic artemisinins, the selected 1,2,4-trioxolane drug development candidate trioxolane **53**, also known as OZ277 or RBx-11160 (Fig. 12) offers significant advantages, including structural simplicity, and a cost-effective, scalable economically feasible and scalable synthesis. To avoid the synthesis of chiral analogues of the trioxolane prototype, the author employed 4-substituted cyclohexanones, which when reacted with symmetrical *O*-methyl-2-adamantanone oxime *via* Griesbaum co-ozonolysis, yield only two achiral diastereomers (*cis* and *trans*). Two key trioxolane intermediates were efficiently synthesized using the Griesbaum co-ozonolysis reaction on a 100 mmol scale, achieving yields of 68% to 78%. Notably, without the need for chromatography purification, X-ray crystallographic analyses of trioxolane **53** and the phthalimide precursor of trioxolane **54** confirmed that the peroxide linkage adopts an axial orientation, while the substituent is equatorially positioned, thereby confirming *cis*-configuration. As exemplified by trioxolanes **53–55** (Fig. 12), a series of relatively polar trioxolane derivatives were synthesized through a variety of post-ozonolysis transformations, demonstrating the versatility and modularity of this synthetic platform.

11. Efficient, stereocontrolled synthesis of trioxolanes for ferrous iron-dependent drug delivery

A stereocontrolled, three-step synthesis of 1,2,4-trioxolanes bearing the critical 3-substitution pattern required for ferrous iron-dependent drug activation has been developed,[43] affording the product in 67–71% overall yield. The key transformation is a diastereoselective Griesbaum co-ozonolysis, which predominantly yields trioxolanes in a *trans* relationship between the 3-substituent and the peroxide bridge. This stereochemistry was confirmed by X-ray crystallographic analysis of a representative 3-substituted 4-nitrobenzoate analogue.

An effective strategy for relative stereochemistry in the formation of the trioxolane ring involves Griesbaum co-

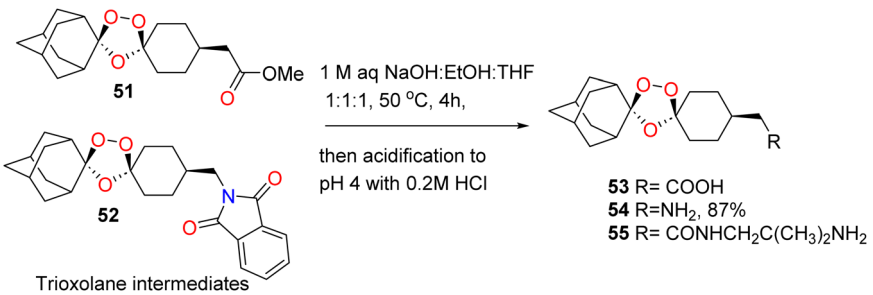

Fig. 12 Synthesis of trioxolanes **53–55**.

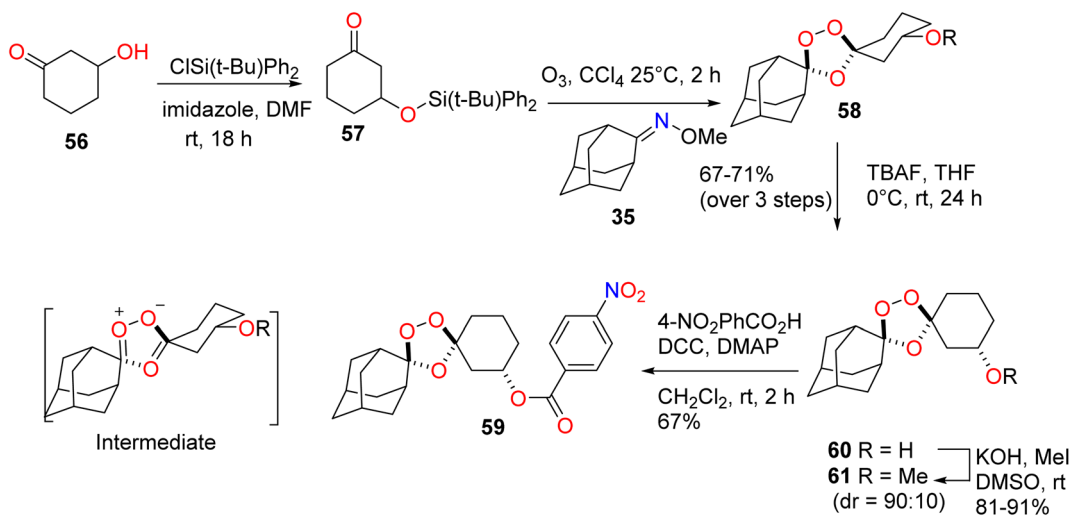

Fig. 13 Stereocontrolled synthesis of the 3-substituted cyclohexane derivative.

ozonolysis, which culminates in a stereochemistry-defining [3 + 2] cycloaddition between a carbonyl oxide and ketone. Vennerstrom and co-workers demonstrated that in 4-substituted cyclohexanones, this cycloaddition occurs preferentially *via* axial attack of the carbonyl oxide, yielding a product comprising equatorial 4-substituents and a *cis* relationship to the axial peroxide.

By analogy, an axial attack on a 3-substituted cyclohexanone is expected to furnish trioxolanes with equatorial 3″ substituents in a *trans* relationship with the peroxide bridge (Fig. 13). To investigate this, *tert*-butyldiphenylsilyl ether **57** was synthesized and subjected to Griesbaum co-ozonolysis with 2.5 equivalents of oxime **11** in CCl_4, affording the trioxolanes **58** in high yield. Subsequently, treatment with TBAF in THF provided alcohol **60**, completing a three-step sequence from precursor **56** in 67–71% overall yield. The ^{1}H NMR analysis of **58** and **60** suggested high diasteroselectivity, which was further confirmed through conversion to methyl ether **61**. Integration of the methoxy signal in the proton NMR spectrum of **61** indicated a diastereomeric ratio of 90 : 10 d.r., confirming the stereochemical outcomes of the Griesbaum cycloaddition.

11.1 Synthetic strategy towards anti-malarial ozonide *via* Griesbaum co-ozonolysis

Using a modified procedure, keto phenol **62** was transformed into ketoepoxide **63** with an 87% yield.[44] Griesbaum co-ozonolysis of **63** with *O*-methyl-2-adamantanone oxime **53** afforded epoxy ozonide **64** (54%) yield. Subsequently, treatment of **64** with morpholine followed by mesylate furnished compound **65** in 60% yield (Fig. 14).

Griesbaum co-ozonolysis of keto acetate **66** with fluorinated *O*-methyl-2-adamantanone oximes **67** and **68** (ref. 45) afforded the corresponding ozonide esters **69** (54%) and **70** (44%), respectively (Fig. 15). These intermediates were then subjected to a one-pot acetate hydrolysis and alkylation with *N*-(2-chloroethyl)morpholine, followed by mesylate salt formation, yielding fluorinated ozonides **71** and **71** in overall yields of 77% and 72%, respectively.

Ozonide **71** was obtained as a 1 : 1 mixture of diastereomers. Chlorosulfonylation of ketone yielded crude **73** (10%) yield, which was subsequently converted into the corresponding pentafluorosulfonate ester **75** (70%) (Fig. 16).

Griesbaum co-ozonolysis of pentafluorosulfonate ester **75** prepared from ketone **73** chlorosulfonylation (10%) and subsequent fluorination (70%) (Fig. 16), with *O*-methyl-2-adamantanone oxime **35**, afforded the corresponding perfluorosulfonyl substituted ozonide.

11.2 Desymmetrized anti-malarial trioxolanes: synthesis and *in vivo* profiling

To expand upon the earlier investigation of *trans*-3″ carbamates-containing trioxolanes,[46] both enantiomeric forms of the newly designed analogues were synthesized and evaluated. This included the preparation of the (*S*,*S*) diastereomers of

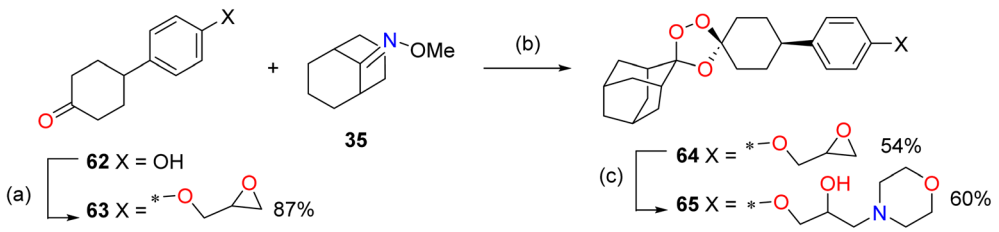

Fig. 14 Stereoselective ozonide derivative synthesis.

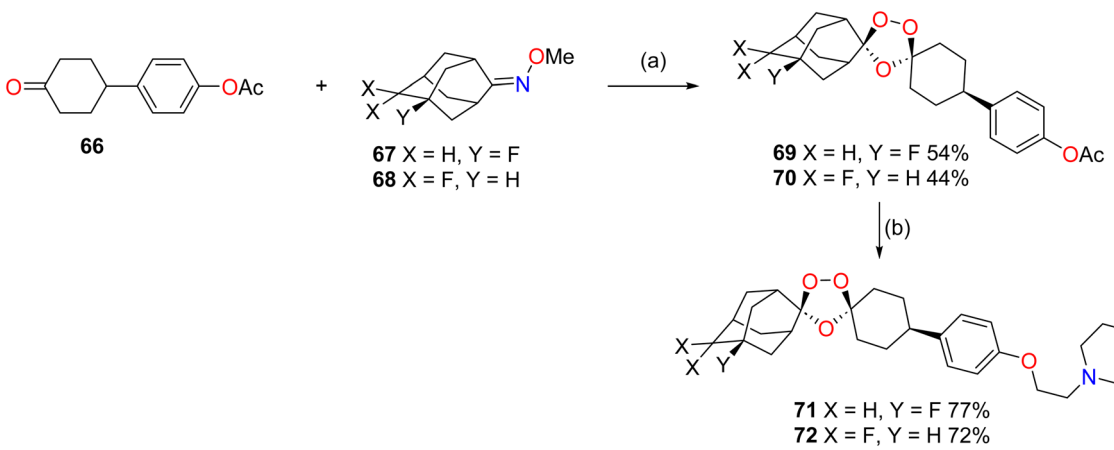

Fig. 15 Synthesis of fluorinated ozonide.

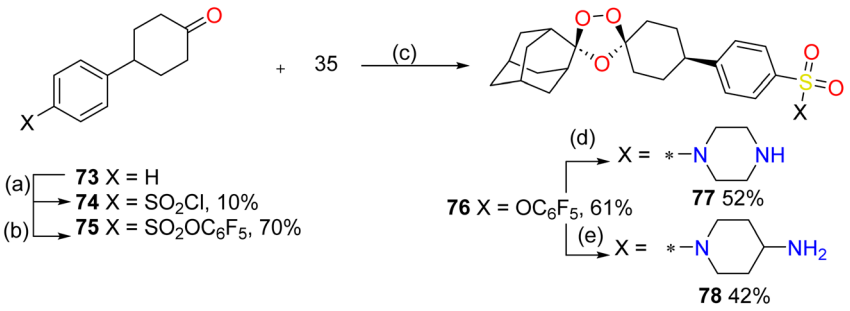

Fig. 16 Synthesis of *p*-sulfonyl phenyl ozonide derivatives.

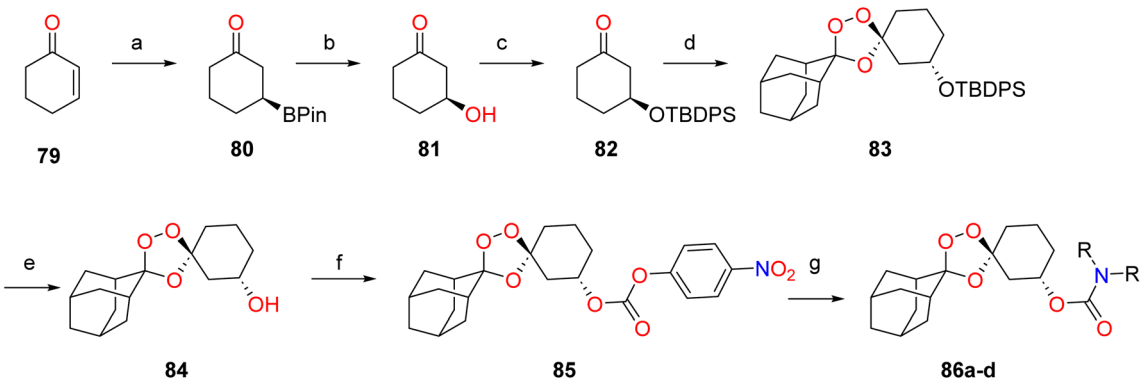

Fig. 17 Representative enantiocontrolled synthesis of (*R*,*R*)-*trans*-3″ analogues **86a–d**.

compounds that had previously been accessed only as (*R*,*R*) forms. To this end, the (*S*,*S*) *trans*-3″ analogues were synthesized *via* an enantioselective route, beginning with a (*R*)-taniaphos-mediated asymmetric borylation of cyclohexanone, which provided the chiral boronic ester intermediate bearing the desired *S*-configuration. This stereochemically defined intermediate laid the foundation for subsequent stereocontrolled elaboration into the target (*S*,*S*)-configured trioxolane carbamates. Both enantiomers of the new analogues were studied, and the (*S*,*S*) forms were prepared for analogues earlier available only as (*R*,*R*). Thus, (*S*,*S*) *trans*-3″ analogues were synthesized in an enantiocontrolled fashion, starting with (*R*)-taniaphos-mediated asymmetric borylation of cyclohexenone to prepare intermediate **80**.

Oxidation of the C–B bond in intermediate **80**, followed by protection of the resulting alcohol as a TBDPS ether, furnished ketone **82**. This intermediate underwent a diastereocontrolled Griesbaum co-ozonolysis with adamantan-2-one *O*-methyl-oxime, affording the *trans*-trioxolane intermediate **83** in a 12 : 1 diastereomeric ratio (d.r.), as determined by ^{1}H-NMR analysis. Subsequent TBDPS deprotection of **83**, followed by conversion to the corresponding *p*-nitrophenyl carbonate **85**, enable late-stage diversification *via* carbamate formation to yield the desired (*S*,*S*)-*trans*-3 carbamate analogues **86a–d**. An analogous enantioselective sequence, employing the enantiomeric taniaphos ligand, was used to access the complementary (*R*,*R*)-*trans*-3-carbamates analogues **86a–d** (Fig. 17).

12. Effect of functional group polarity on the anti-malarial activity of spiro and dispiro trioxolanes

In this study,[47] physicochemical characterization and antimalarial evaluation of structurally diverse derivatives were reported based on early trioxolane scaffolds, encompassing a broad range of polarity. The polarity objective was to determine which functional groups contributed to favorable antimalarial activity, and to identify lead compounds exhibiting an optimal balance between lipophilicity (log *P*/log *D*) and aqueous solubility. A key emphasis was placed on the carboxylic acid moiety due to its twofold benefits: its capacity to generate water-soluble salts and its therapeutic relevance demonstrated by semisynthetic artemisinin derivatives such as artesunate and artelinate.[48]

Trioxolanes **93** (50%), **94** (18%), **95** (25%), **96** (45%), and **99** (49%) were synthesized directly *via* Griesbaum co-ozonolysis involving the reactions of *O*-methyl-2-adamantanone oxime **87** with either 4-substituted cyclohexanones **88** or benzophenones **89**. The corresponding trioxolane carboxylic acids **91** (58%), **95** (84%), **22** (90%), diol **90** (46%), alcohol **92** (87%), and diamine **99** (29% overall) were obtained through aqueous KOH hydrolysis of their respective trioxolane ester precursor. These ester precursors were themselves synthesized directly by co-ozonolysis, yielding between 25–63%. The synthesis of compound **92** required three additional post-ozonolysis

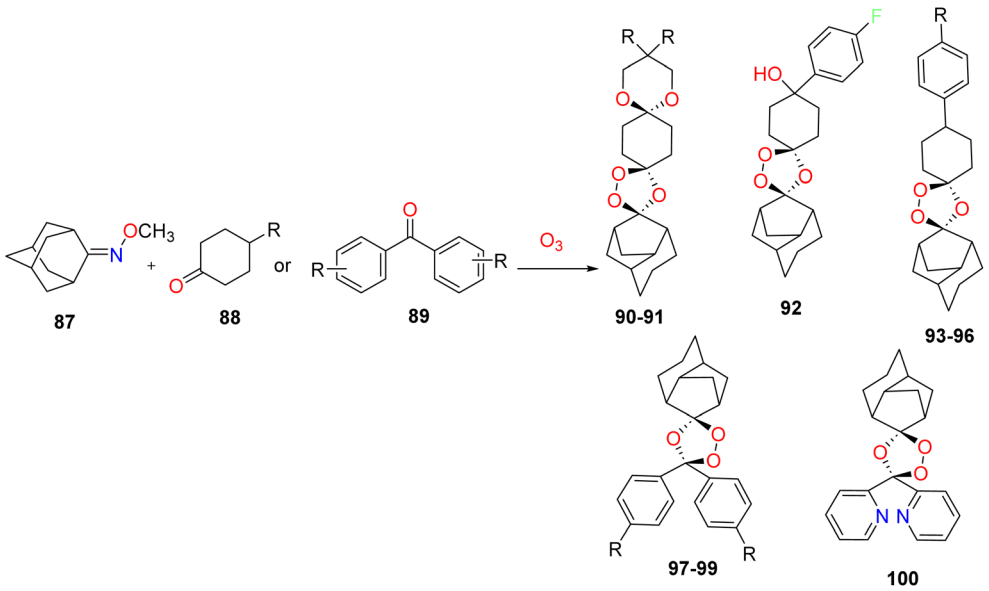

Fig. 18 Griesbaum co-ozonolysis reaction to prepare spiro and dispiro-1,2,4-trioxolanes.

transformations: reduction using lithium borohydride or lithium triethyl borohydride for **92**, phthalimide formation *via* the Mitsunobu reaction, and hydrazinolysis for phthalimide deprotection (Fig. 18).

13. Characterization of major CYP450 metabolites of ozonide OZ277

In 2008, L. Zhou[49] reported the synthesis of the minor metabolite **G** *via* a four-step sequence (Fig. 19), starting with a Griesbaum co-ozonolysis reaction between 5-acetoxy-2-adamantanone *O*-methyl oxime **101** and keto ester **102**. Oxime ether **101** was prepared in two steps: initially by the reaction of 5-hydroxy-2-adamantanone with methoxylamine HCl and pyridine (yield: 97%), followed by acetylation with acetic anhydride, pyridine, and catalytic DMAP (yield: 91%). The ozonolysis of unsymmetrical oxime ethers such as **101** generates enantiomeric carbonyl oxide intermediates, which can undergo cycloaddition reactions with 4-substituted cyclohexanones **102** to potentially yield four isomeric ozonides.[50] Based on previously established data, the formation of two major ozonide isomers was anticipated, with substituent and peroxo groups adopting equatorial and axial orientations, respectively, in the cyclohexane ring. Indeed, analysis of the crude reaction mixture (30%, silica gel chromatography, 10% ether in hexanes) using ^{1}H and ^{13}C NMR revealed two predominant ozonide diester isomers, from which the major isomer **103** was isolated by crystallization in 17% yield. The *trans*, *cis* configuration was assigned based on the conversion of the *trans*, *cis* ozonide diester **103** to **105** (86%).

Similarly, the major metabolite **106 F** was synthesized *via* a parallel four step sequence (Fig. 19), starting from a Griesbaum co-ozonolysis between 5-(4-methylbenz oxy)-2-adamantanone *O*-methyloxime and keto ester **102**, which upon chromatography purification afforded a mixture of four ozonide diester diastereomers (**103** and **104**). The oxime ether precursor was synthesized by benzoylation of 5-hydroxy-2-adamantanone using 4-methylbenzoyl chloride in pyridine (90%), followed by conversion to the *O*-methyloxime using methoxylamine hydrochloride pyridine (94%).

The 4-methylbenzoate group was strategically chosen over acetate to increase the molecular weight, facilitating fractional crystallization of the minor ozonide diester isomers, and to provide distinct benzylic singlet proton NMR signals for effective diastereomer discrimination. Repeated chromatography

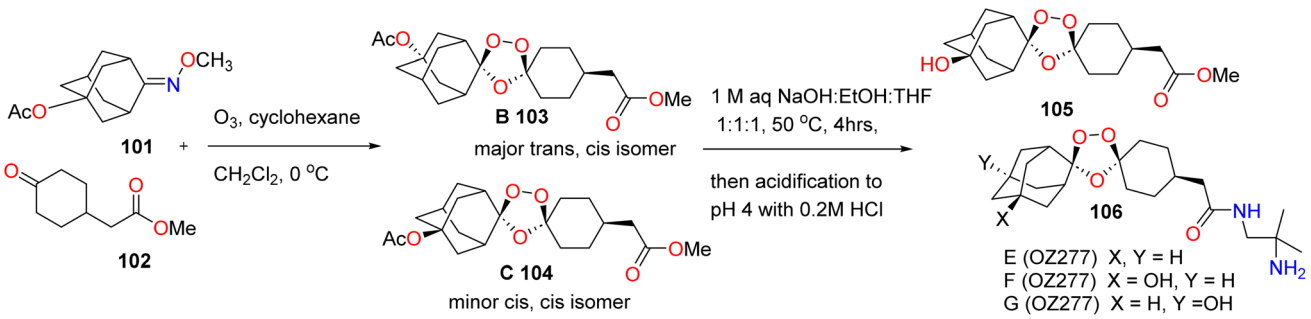

Fig. 19 Synthesis of ozonide diester diastereomers.

yielded four fractions of isomers. Crystallization of the isomer from acetone afforded **103** as colorless crystals, whose *trans cis* diastereomeric structure was confirmed by X-ray crystallographic analysis.

14. SAR of an ozonide carboxylic acid (OZ78) against *Fasciola hepatica*

Following the method of Tsandi,[51] acyl sulfonamides were synthesized by coupling with methanesulfonamide in the presence of DMAP and DCC. Corresponding hydrazides were obtained *via* direct reaction of the methyl ester with hydrazine. Glycine and taurine conjugates of ozonides were prepared by coupling the HOBt activated ester[52] with glycine ethyl ester and taurine, respectively.

Ozonide dicarboxylic acid **109** was synthesized through five-step sequence starting from compound **107**, the Knoevenagel condensation product of 1,4-cyclohexanedione monoethylene ketal and isopropylidene malonate (Fig. 20).[53] Subsequently, reduction (99%), deketalization (27%), and esterification (37%) yielded diester ketone **108**, which underwent Griesbaum co-ozonolysis with oxime ether **35** (ref. 54) to give diester ozonide **109** in 75% yield. Hydrolysis of **109** furnished the target dicarboxylic acid **50** in high yield.

15. Machines *vs.* malaria: flow synthesis of anti-malarial candidate OZ439

Processing conditions for the Griesbaum co-ozonolysis were optimized using commercially available 4-phenylcyclohexanone **66** as a model substrate.[55,56] A solution oxime **11** and ketone **66** (X = H) in EtOAc was exposed to an ozone stream, with both liquid and gas flow rates adjusted to maximize the product yield.[57] Using an excess of ketone gave moderate yields, whereas using an excess of oxime significantly improved the outcome, affording compound **68** in 76% isolated yield after purification (Fig. 21). The continuous flow reaction ran smoothly for 45 min; however, extended reaction times led to blockages due to slight solvent evaporation.

This issue was resolved by reducing the concentration of oxime **35** (0.4 to 0.2 M) and ketone **110** (0.2 to 0.1 M), while increasing the flow rates of both liquid (1 mL min^{-1}) and gas (1 L min^{-1}), to maintain system throughput. Under these diluted conditions, the reaction proceeded continuously for over 3 hours without clogging, resulting in 78% yield and a throughput of 1.6 g h^{-1} (38.4 g d^{-1}).

The same reactor setup was successfully applied to the co-ozonolysis of **35** and **110**, delivering the 1,2,4-trioxolane **111** in 70% yield with 9 : 1 *cis*/*trans* selectivity. This corresponded to a production rate of 1.9 g h^{-1} (45.6 g d^{-1}). Notably, this continuous flow protocol offers advantages over batch ozonolysis by enhancing safety and efficiency, and eliminating the use of flammable solvents such as pentane through substitution with ethyl acetate.

A robust and efficient machine-assisted protocol was developed for the synthesis of the anti-malarial drug candidate OZ439,[58] leveraging flow chemistry to overcome limitation batch processing. Three key transformations (selective partial hydrogenation, phenolic acetylation, and Griesbaum co-ozonolysis) were successfully adapted to continuous flow conditions, enabling improved process control, safety, and scalability. Notably, this new synthetic route avoided the use of the genotoxic reagent 4-(2-chloroethyl)morpholine, offering a safer and more sustainable alternative for large scale production.

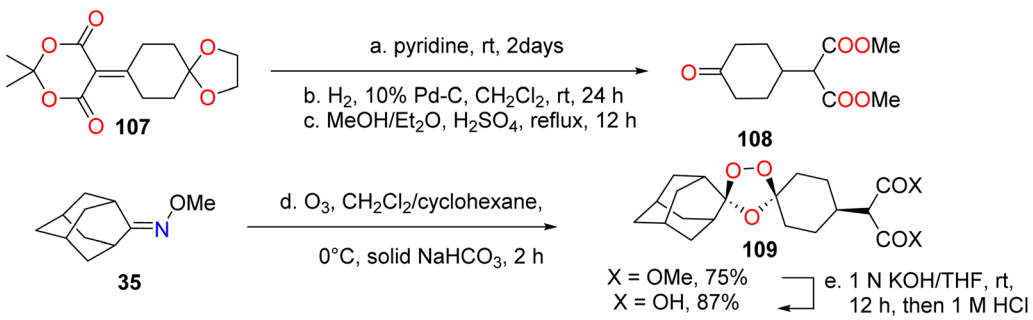

Fig. 20 Five-step synthesis of diester ozonide and diacid ozonide.

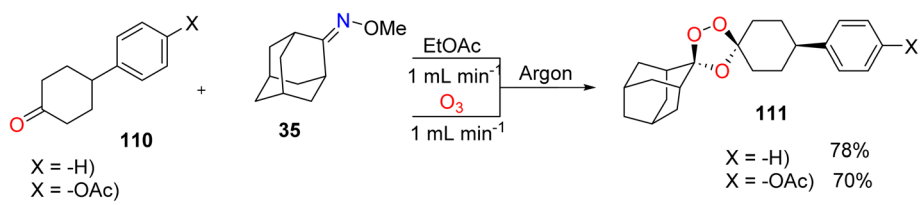

Fig. 21 Flow setup for ozonide formation.

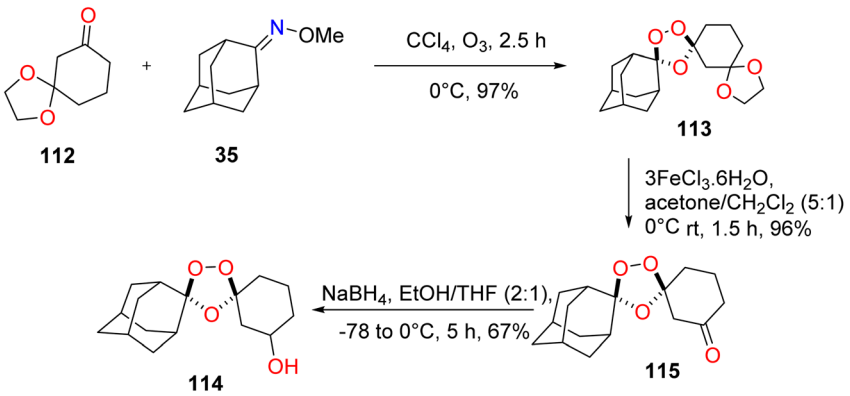

Fig. 22 Synthesis of the 3-keto trioxolane alcohol derivative.

16. Targeted drug delivery to malaria parasite using an arterolane-like scaffold

Gratifyingly, the partially protected diketone **112** underwent efficient Griesbaum co-ozonolysis with *O*-methyl-2-adamantanone oxime **11**, yielding the desired trioxolane **113** in nearly quantitative yields (Fig. 22). The use of two or more equivalents of oxime was critical for achieving high conversion. Subsequently, deprotection of ketal moiety **113** using ferric chloride hexahydrate in acetone/dichloromethane proceeded smoothly, affording ketone **115** in excellent yield. A modified reduction protocol, based on conditions previously reported for 4-keto trioxolanes, was successfully applied to reduce 3-keto trioxolane **115**, yielding alcohol **114** in 67%. The reduction showed minimal diastereofacial selectivity, producing a roughly 1 : 1 mixture of *cis* and *trans* racemic diastereomers.

This work[59] presents an improved chemical scaffold for trioxolane-mediated drug delivery supported by the efficient, concise, and scalable synthesis of key intermediate **114**, which will facilitate further exploration of this class of compounds. Additionally, the amino nucleoside was employed as a chemical biological probe to monitor drug release in *P. falciparum*, demonstrating the utility of this approach. The use of puromycin as a drug surrogate is anticipated to enable future studies on trioxolane-mediated drug delivery across malaria and other disease models.

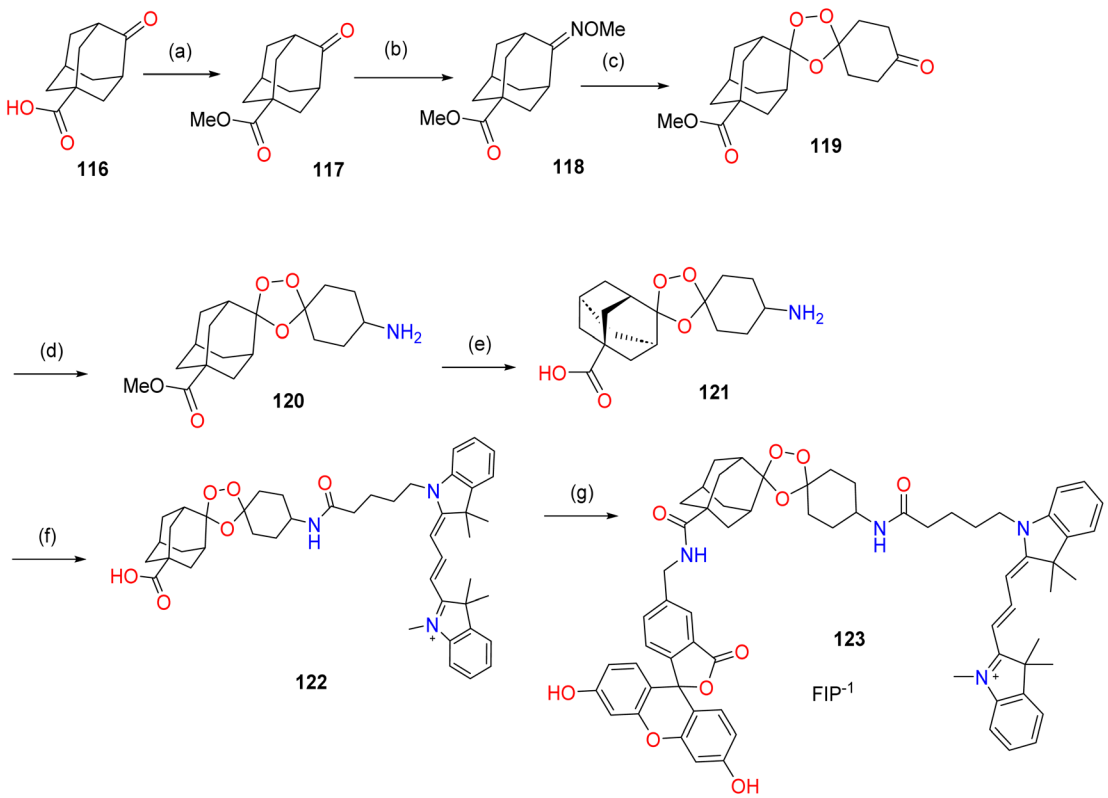

Fig. 23 Synthetic route of FIP^{-1}.

17. Endoperoxide-based FRET probe for ratiometric imaging of labile iron in living cells

The design, synthesis, and biological evaluation of FRET Iron Probe 1 (FIP^{-1}) was reported in ref. 60, as a reactivity-based probe for ratiometric fluorescence imaging of labile Fe(II) pools in living systems. Inspired by antimalarial natural products and their mechanisms of iron-dependent activation, FIP^{-1} incorporates two fluorophores, fluorescein (donor) and CY3 (acceptor) linked *via* an Fe(II)-cleavable endoperoxide bridge that is disrupted upon activation, separating the fluorophores and reducing FRET. FIP^{-1} exhibits high selectivity for Fe(II) over other metal ions in aqueous buffer and enables dynamic visualization of intracellular iron fluctuation under iron supplementation or chelation conditions.[61–64]

The synthesis of FIP^{-1} involves the five-step preparation of a dual-functionalized adamantyl-endoperoxide linker from commercially available starting materials (Fig. 23). Starting with 2-adamantanone-5-carboxylic acid **116**, Fischer esterification yields the methyl ester **75**, which was subsequently converted to oxime ether **118** *via* reaction with hydroxylamine hydrochloride.[65,66] Compound **118** underwent Griesbaum co-ozonolysis with 1,4-cyclohexanedione and ozone to afford endoperoxide **119**. Reductive amination of **119**, followed by saponification, provided the carboxylic acid-functionalized endoperoxide linker **121**. Separately, Cy3-NHS-ester and 5-AMF were synthesized according to a previously published procedure.[43] These fluorophores were then subsequently coupled to linker **121** to furnish the final ratiometric probe FIP^{-1} **123**.[67]

18. Expanded scope of Griesbaum co-ozonolysis for structurally diverse ferrous iron sensors

Sterically shielded 1,2,4-trioxolanes, synthesized *via* Griesbaum co-ozonolysis, have emerged as key scaffolds in the development of chemical probes for detecting labile ferrous iron. Another report[68] optimized co-ozonolysis conditions that proceeded with high efficiency diastereoselectivity across a broader substrate scope, enabling the design of next-generation iron ferrous sensors with tailored reactivity and physicochemical properties.

When cyclic ketone and oxime are employed as co-reactants, the resulting trioxolane adducts exhibit notable stability, attributed to steric shielding of the endoperoxide bond by an adjacent axial C–H bond rigid carboxylic framework. Vennerstrom and co-workers exploited this effect in the development of the antimalarial agents arterolane[69] and artefenomel,[70] where the adamantane-derived trioxolane core stabilized the peroxide moiety, enhancing its selective reactivity with labile Fe(II) in *Plasmodium* parasites. This Fenton-type activation mirrors the mechanism of artemisinin derivatives, underscoring the therapeutic relevance of peroxide stability and iron-triggered activation. Growing recognition of labile iron as the bioavailable intracellular iron pool has driven the development of oxidation-state specific probes, primarily *via* reactivity-based strategies.[71] Ferrous iron-triggered reduction of N–O or O–O bonds enables the activation of fluorophores (*e.g.* TRX-FIP-1 (ref. 72)), modulation of FRET pairs (TRX-FRET), release of tethered reporters (*e.g.* TRX-PURO,[73] ICL-1,[74] HNG[75]), or covalent capture of PET radiolabels (18F-TRX[76,77]). Trioxane and trioxolane-based reagents have also found utility in chemoproteomic profiling of malarial parasite and mammalian cancer

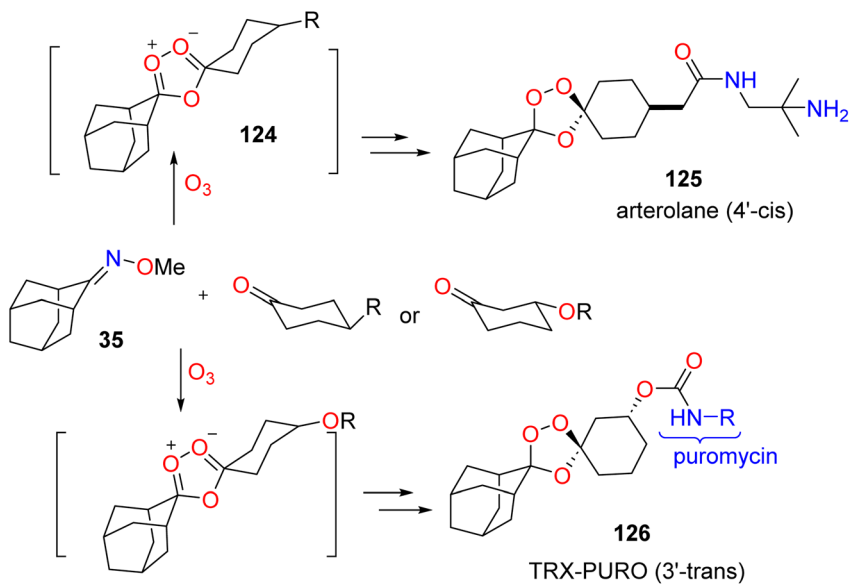

Fig. 24 Conversion of oxime to carbonyl oxide, followed by diastereoselective reaction with the ketone co-reactant, with axial addition favored.

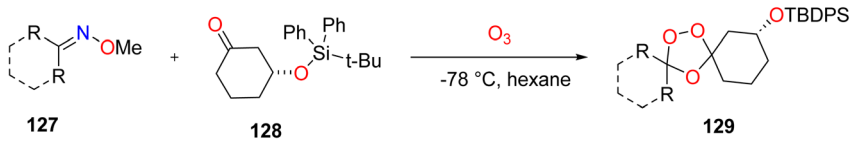

Fig. 25 Scope of Griesbaum co-ozonolysis involving structurally diverse oxime **127** and ketone **128**.

cells (*e.g.* FIPC-1 (ref. 78)), further demonstrating their versatility in bioanalytical applications (Fig. 24).

While arterolane-like pharmacophores have played a central role in the design of first-generation ferrous iron probes, further optimization will likely require access to trioxolane scaffolds with expanded iron reactivity profiling and improved physiochemical properties that are suitable for *in vivo* applications. The Griesbaum co-ozonolysis was revisited as a strategy to access new structural frameworks for ferrous iron-reactive therapeutics and chemical probes. Mechanistically, the Griesbaum co-ozonolysis proceeds *via* [3 + 2]/retro-[3 + 2] sequence, wherein *O*-methyloxime undergoes ozonolysis to generate a carbonyl oxide intermediate. This transient then engages in stereochemistry determining [3 + 2] cycloaddition with a ketone to form the 1,2,4-trioxolane adducts. The reactions between adamantane-derived oximes and substituted cyclohexanones are known to favor axial attack of the carbonyl oxide on the ketone, typically furnishing *cis*-40 or *trans*-30 configured trioxolanes with useful diastereoselectivity (d.r. 9 : 1) (Fig. 22).[54]

Initial reports by Griesbaum primarily focused on simple alkyl and cycloalkyl substrates, while subsequent studies have emphasized adamantane-derived oximes, which yield pharmacologically active trioxolanes.[79] Other groups have extended this chemistry to non-adamantane substrates.[80,81] An optimized Griesbaum co-ozonolysis protocol was previously reported, employing adamantanone oxime as the access reagent and using the ketone as the limiting component, which afforded hydroxy trioxolanes (70% yield) at 0 °C in CCl_4. However, this

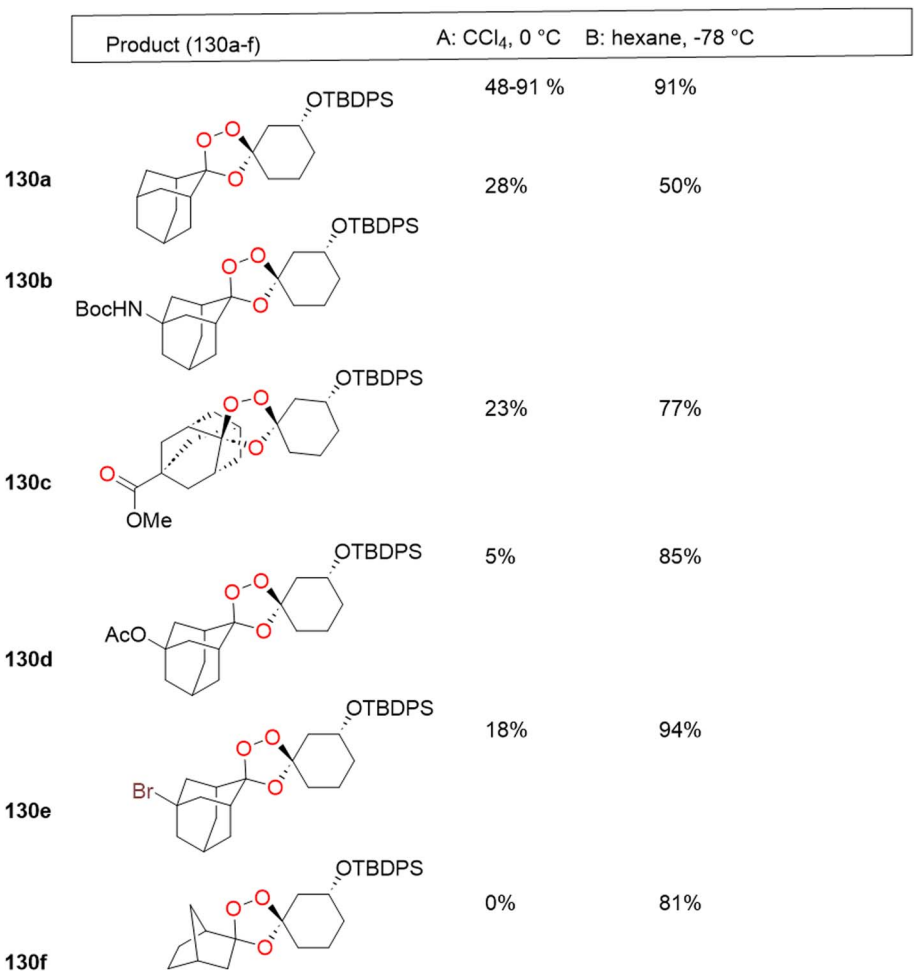

Fig. 26 Structures of adducts **130a–f** with their respective yields in conditions A and B.

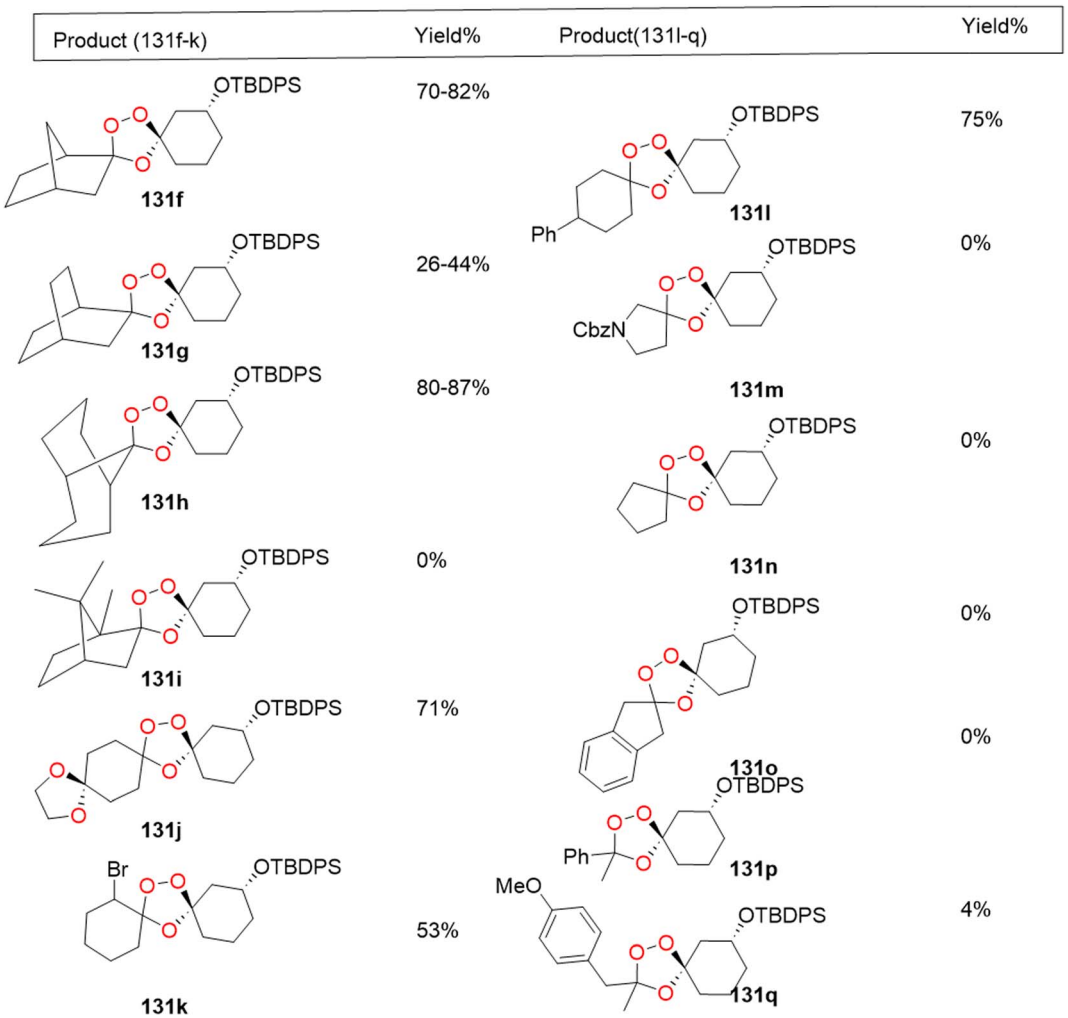

Fig. 27 Structures of trioxolane adducts **131f–q** and their yields.

method was found to be inadequate for substituted adamantanes, and particularly non-adamantyl ketones, where the yield decreased to 5–23%, or reactions failed altogether. These poor outcomes were attributed to possible side-reactions involving ozone or the carbonyl oxide intermediate (Fig. 25). To address these limitations, subsequent studies investigated the co-ozonolysis of enantiopure ketone **128** [82] with various substituted adamantanone oxime **127** under low temperature conditions (−78 °C in hexanes, O_3, flow 6 g h^{-1} or 1.1 L per min O_2). These revised conditions (condition B) yielded substantial improvement: compound **130a** was isolated in 77–94% yield (*vs.* 48–91% under previous conditions), and substituted trioxolanes **130b–e** were obtained up to 94% yield. Diasteroselectivity was also improved, with exclusive formation of the *trans* isomers for **130a–e** under condition B compared to 90 : 10 d.r. under the original conditions. Notably, no diastereofacial selectivity was observed when unsymmetrical carbonyl oxides were employed.

Given the role of axial C–H shielding in modulating the Fe(II)-specific Fenton reactivity of endoperoxide probes (*e.g.* TRX-PURO, ICL-1),[72] other bicyclic aliphatic ring systems have been evaluated computationally for potential steric shielding effects. The ring system including bicycle[2.2.1]heptane, bicycle[2.2.2]heptane, and bicycle[3.3.1]nonane were identified as promising candidates. Applying condition B, co-ozonolysis of bicycle[2.2.1]heptan-2-one methyl oxime with **128** afforded troxolan **130f** in 81% as a mixture of stereoisomers (13 : 8 : 1 by ^{1}H NMR). Notably, this transformation failed under the original condition A. Building on these results, more oxime substrates were tested at low temperature (Fig. 26), which expanded the range of trioxolane adducts that could be obtained.

Under the optimized low temperature conditions, the reaction of ketone **128** with bicyclo[2.2.2]octan-2-one methyl oxime and bicyclo[3.3.1]nonan-9-one methyl oxime yielded trioxolane adduct **131g** and **131h** in modest (26–44%) and excellent (80–87%) yields, respectively. In contrast, camphor methyl oxime failed to afford adduct **131i**, likely due to steric hindrance around the oxime moiety. Further substrate exploration included substituted cyclohexanone, cyclopentanone, and acyclic oximes. Cyclohexanone-derived oximes with 4-substitution provided adducts **131j** and **131l** in 71% and 53% yields, respectively, while 2-bromocyclohexan-1-one methyl oxime

afforded **131k** in 53% yield. Unexpectedly, cyclopentanone oxime gave **131k** in 53% yield. Notably, cyclopentanone oximes failed to yield quantities of the expected trioxolane adducts (**131m–o**), likely due to unfavorable ring strain or instability of the corresponding intermediates under the reaction conditions (Fig. 27).

The failure of certain Griesbaum co-ozonolysis reactions may be attributed to intrinsic instability of the resulting trioxolane adducts, or competitive side reactions of the carbonyl oxide intermediate, such as dimerization. For example, attempts to form trioxolanes **131p** and **131q** from methyl oximes of acetophenones and 4-methoxyphenylacetone, respectively, yielded no isolable products (Fig. 27).

To assess the Fe^{2+}-dependent reactivity of selected novel trioxolanes like **131f**, **131g**, and **131h**, their incorporation into payload-bearing trioxolane conjugates has been investigated. As a surrogate for physiological Fe^{2+} reactivity, these studies evaluated their ability to undergo iron(II)-triggered payload.[83,84] Conjugates bearing mefloquine as the payload exhibited potent *in vitro* anti-plasmodial activity, with IC_{50} values of 74 nM and 24 nM, comparable to the positive control ($IC_{50} = 17$ nM). These findings support a canonical Fenton-type activation mechanism,[85] wherein Fe(II)-mediated cleavage of the trioxolane ring triggers payload release, thereby accounting for the observed anti-malarial potency of the conjugates.

19. Targeting ferrous iron mobilization in *Pseudomonas aeruginosa via* Iron(II)-caged LpxC inhibitor

To realize the proposed disconnection, synthetic access to both the LpxC inhibitor (LpxCi) carboxylate and an aminooxy-functionalized trioxolane (TRX) intermediate was required (Fig. 28).[86] The LpxCi carboxylate corresponded to a late-stage intermediate in the synthesis of hydroxamate-based inhibitors, while the TRX component was designed to enable site-specific conjugation *via* the hydroxamate oxygen. Following extensive optimization, a robust and scalable synthetic route was established that enabled multigram scale production of the trioxolane hydroxamate conjugates. This strategy provides a versatile platform for constructing iron(II) response drug conjugates, expanding the utility of trioxolane scaffolds for targeted delivery applications.

The synthesis of the aminooxy-functionalized trioxolane intermediate (±)-**138** was achieved *via* a streamlined route (Fig. 28). Monobenzylation of cyclohexane-1,3-diol yielded ether **133**, which underwent a Mitsunobu reaction with *N*-hydroxyphthalimide to afford intermediate **134**. Subsequently benzyl deprotection of $BCl_3 \cdot SMe_2$ furnished alcohol **135** in 89% yield. Oxidation of **135** to ketone **136** was initially hindered by its tendency to undergo beta-elimination; however, this step was successfully optimized using Dess–Martin periodinane or Swern oxidation under carefully controlled conditions. The resulting ketone **136** underwent Griesbaum co-ozonolysis with the *O*-methyl oxime of adamantan-2-one to afford trioxolane **137** in 92% yield, with diastereoselectivity (13 : 1 d.r) favoring the *trans* isomer, consistent with prior observations.[87]

To assess the *in vivo* stability and pharmacokinetics, compound **140** was administered *via* intraperitoneal (IP) injection to female NSG mice. Plasma samples were analyzed for both intact conjugate **140** and liberated LpxC inhibitor **140** to evaluate potential Fe^{2+}-dependent or-independent release mechanisms. Compound **140** displayed a rapid elimination profile with a half-life ($T_{1/2}$) of approximately 0.7 hours, closely resembling the pharmacokinetics of PF-508109037 (Fig. 29 and 30).

20. Artefenomel regioisomer RLA-3107: a promising lead for the next-generation endoperoxide anti-malarial

The Griesbaum co-ozonolysis reaction, widely employed for the synthesis of 1,2,4-trioxolanes, is intrinsically diastereoselective, typically yielding *cis* or *trans* diastereomers with a 9 : 1

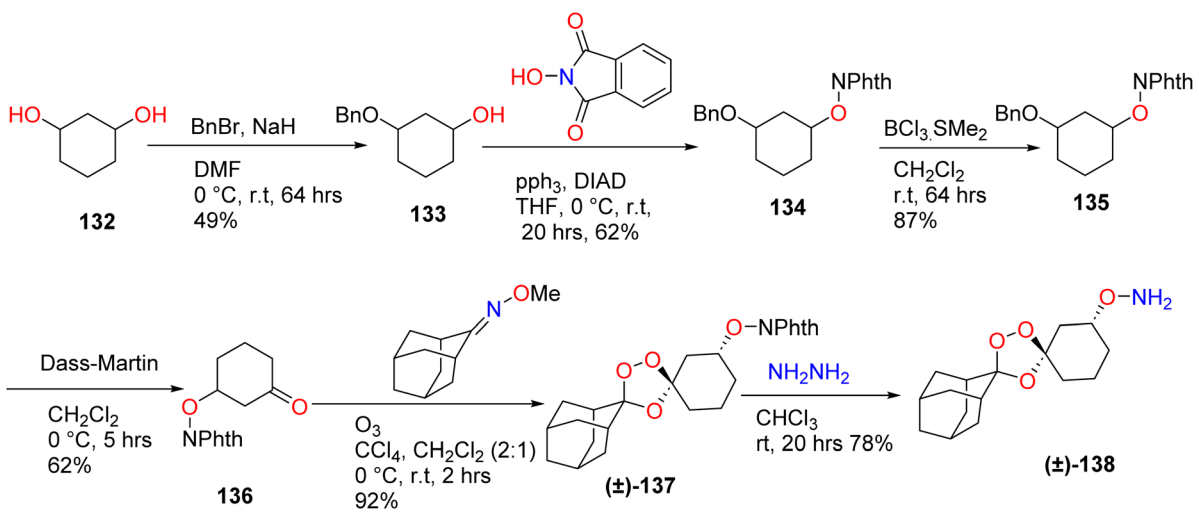

Fig. 28 Stereo-controlled synthesis of key trioxol intermediate, **138**, bearing a 3-aminooxy function.

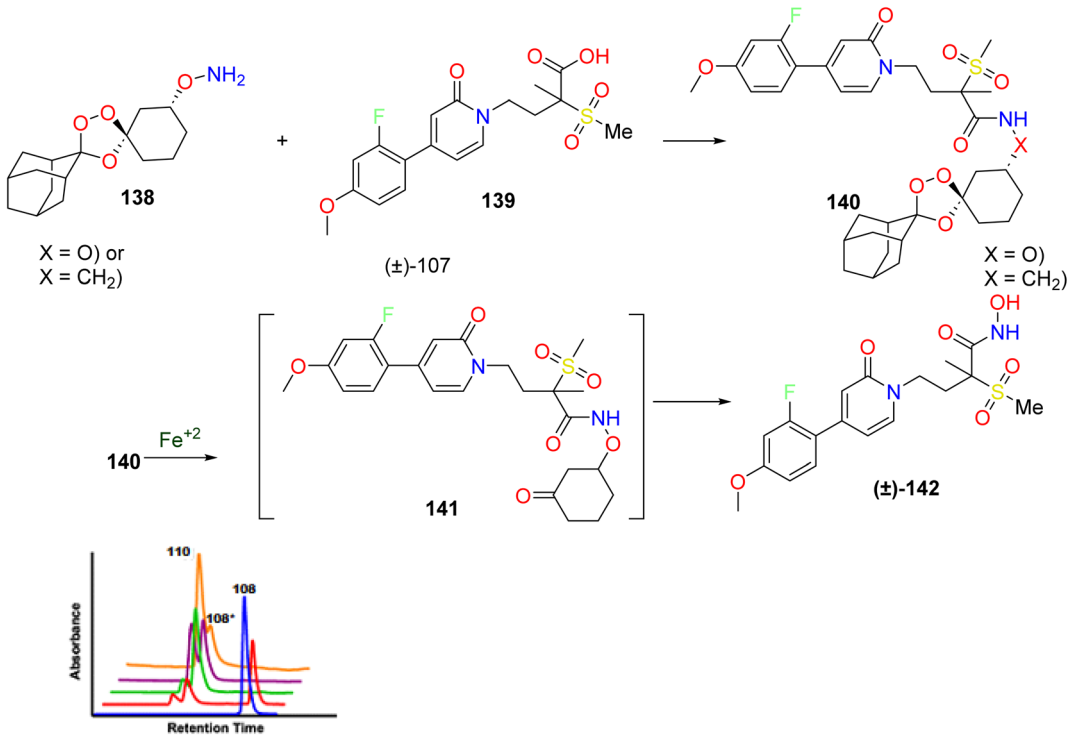

Fig. 29 Synthesis of hydroxamate and amid-linked TRX conjugates from known LpxC inhibitors and reaction of 9 with ferrous ammonium sulfate.

diastereomeric ratio when using C4- or C3-substituted cyclohexanones, respectively. Full stereocontrol can thus be achieved using enantiopure cyclohexanone substrates, as demonstrated in the enantioselective synthesis of arterolane-like *trans*-R4 amide and carbamate, as well in O'Neill's desymmetrized tetraoxanes synthesis.[88] In the present work,[89] racemic cyclohexanone was employed to afford the (±)-**2** *trans* diastereomer as the major product.

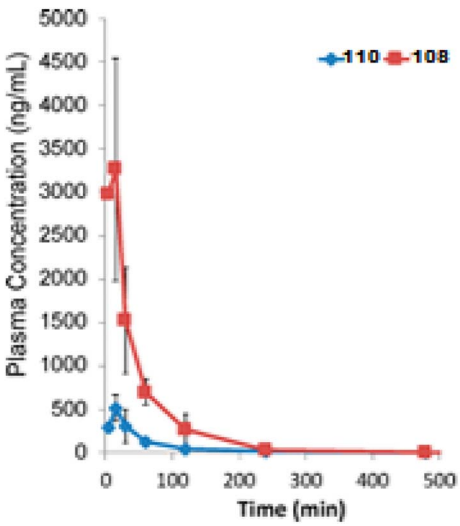

Fig. 30 Plasma exposure profile of prodrug **140** (red) and systematically released **142** (blue).

A stereocontrolled synthesis of RLA-3107 **148**, a regioisomer of the clinical studied drug candidate artefenomel, was accomplished starting with a palladium(II) catalyzed 1,4-conjugate addition. A dicationic palladium(II) complex, formed *in situ* from Pd(acac) and $Cu(BF_4)_2 \cdot H_2O$, effectively catalyzed the 1,4-addition of 4-(acetoxy)phenyl boronic acid to cyclohexen-1-one **144**, affording ketone **145** in 91% yield. Subsequently, Griesbaum co-ozonolysis of **145** with adamantan-2-one *O*-methyl oxime **35** in the presence of ozone at 0 °C yielded 3-aryl substituted 1,2,4-trioxolane intermediate **146** in nearly quantitative yield with a diastereomeric ratio (d.r.) of 8 : 1. Hydrolysis of the acetate protecting group under basic condition (KOH in MeOH/THF at 50 °C) afforded phenol **147** in 95% yield. This intermediate was then alkylated with 4-(2-chloroethyl)morpholine hydrochloride using NaOH and $[(Bu)_4NHSO_4]$ in acetonitrile at 55 °C, furnishing (±)-**148** in 62% yield or (50% overall yield for four steps). Final purification of both **147** and **148** *via* column chromatography removed any residual minor diastereomer, yielding pure *trans* (±)-**148**, as confirmed by ^{1}H NMR analysis. Since the precursor ketone has been previously synthesized in the enantiopure form,[80] this route is fully amenable to enantiomerically synthesizing **116** (Fig. 31).

This work validates the conformational prediction that *trans* 3″-aryl substituted trioxolanes exhibit comparable Fe^{2+} reactivity and anti-plasmodial activity to their C4-aryl regioisomers counterparts. The *in vitro* and *in vivo* studies presented here demonstrate the 3″-aryl trioxolane scaffold as a promising platform for the design of next-generation peroxide antimalarial drugs including RLA-3107. Building on this, a diverse series of

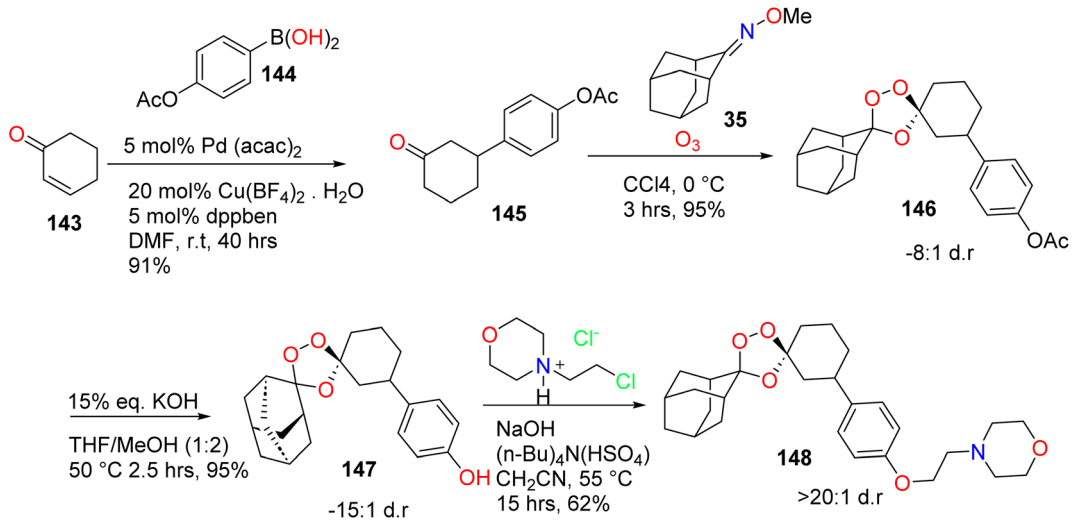

Fig. 31 Stereocontrolled synthesis of artefenomel regioisomers *trans*-(±)-**148**.

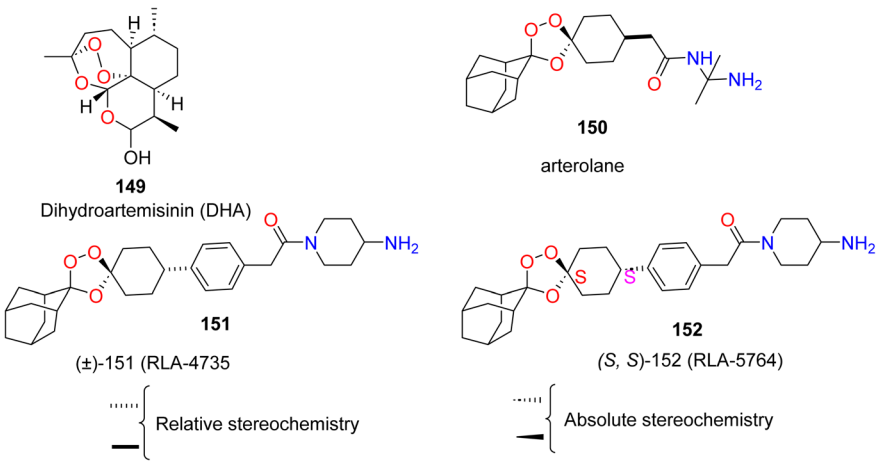

Fig. 32 Structures of dihydroartemisinin, arterolane (**150**), and *trans*-trioxolane analogs (±)-**152** and (*S*,*S*)-**152**, with the stereochemistry indicated.

desymmetrized anti-malarial trioxolanes bearing carbomate side chains was synthesized, targeting both (*R*,*R*) and (*S*,*S*) *trans* isomers. A stereocontrolled synthesis of RLA-3107 (**148**), a regioisomer of artefenomel, was carried out, and conformational analysis confirmed the expected *trans*-3″ stereoisomers. In particular, (*S*,*S*) analogues were accessed *via* enantioselective borylation of cyclohexanone, mediated by (*R*)-taniaphos, to yield the intermediate with a defined *S* configuration. These analogues are currently undergoing biological profiling.

21. Exploration of next-generation trioxolanes among artemisinin analogues

To identify next-generation trioxolane agents with differentiated pharmacological properties, a series of novel analogs bearing the *trans*-4″ substitution inspired by conformational analysis has recently been reported,[90] which predicted stabilization of the endoperoxide bond comparable to that observed with conventional *cis*-4″ substitution. Indeed, congeneric *trans*-4″ analogs of arterolane **150** demonstrated promising antiplasmodial activity in both *in vitro* and *in vivo* models, validating the hypothesis that *trans*-4″ substitution can modulate ferrous iron reactivity in a pharmacologically favorable manner. Continued investigations have led to the identification of compound **152** (Fig. 32), an advanced lead with efficacy against artemisinin-resistant (ART-R) *Plasmodium falciparum* and potential as a trioxolane-based development candidate.

The transition to *trans*-3″ substitution in the 1,2,4-trioxolane pharmacophore introduces two stereogenic centres, giving rise to four possible diastereomers. However, the Griesbaum co-ozonolysis employed for trioxolane synthesis is intrinsically stereoselective, favoring *cis*-4 substitution and *trans*-3″ substitution consistent with prior reports. Leveraging this inherent selectivity, a concise six-step synthetic route was developed to

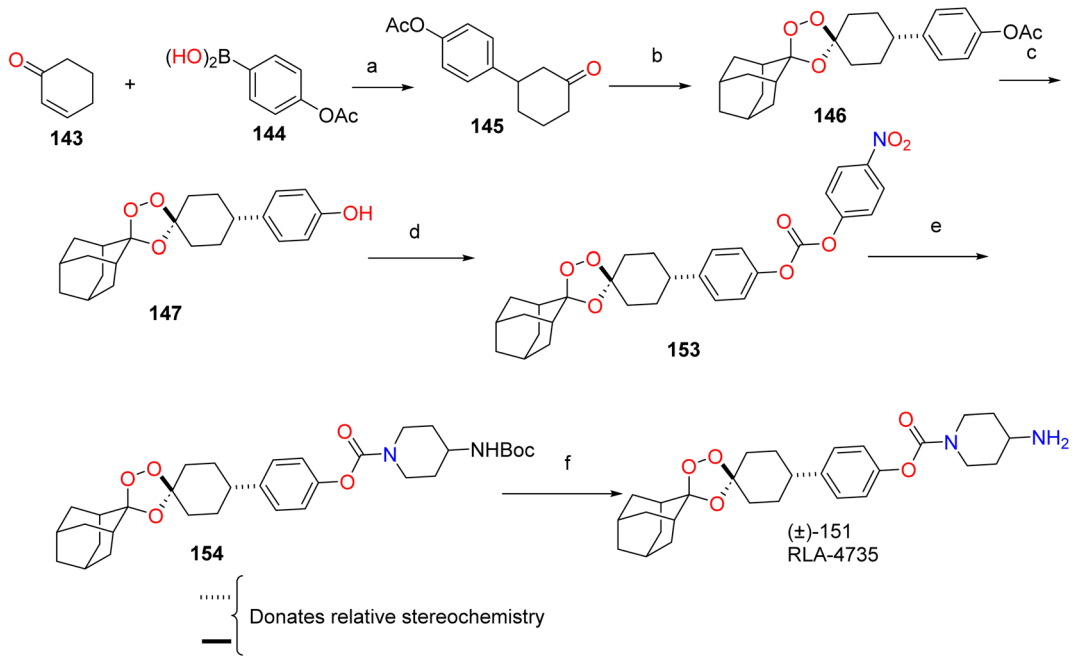

Fig. 33 Synthesis of racemic (±)-**151** (RLA-4735) comprising both (*R*,*R*) and (*S*,*S*).

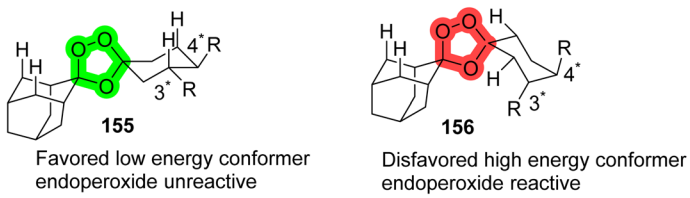

Fig. 34 Iron reactivity of the trioxolane antimalarial is influenced by cyclohexane conformation *cis*-4″ (**155**) and *trans*-3″ (**156**).

access racemic (±)-**152** and related analogs (Fig. 32 and 33), closely aligned with the four-step synthesis previously reported for the artefenomel regioisomer. Access to enantiopure forms, namely (*R*,*R*)-**152** and (*S*,*S*)-**152**, was achieved by simply utilizing enantiomerically pure cyclohexanone intermediates in the Griesbaum reaction.

For the preparation of the (*R*,*R*)-**152** enantiomer, the following conditions were employed: (a) 4-(benzyloxy)phenylboronic acid, 4 mol% acetylacetonatobis(ethylene)rhodium(I), 10 mol% *R*-BINAP, aqueous KOH, dioxane, 100 °C, 16 hours, 54%. For the corresponding (*S*,*S*)-**152** enantiomer, the reaction was performed using *S*-BINAP under otherwise identical conditions, affording the desired product in 33% yield.

These finding underscore the therapeutic potential of (*S*,*S*)-**151** and structurally related, further optimized analogs for the treatment of both artemisinin-sensitive and artemisinin-resistant (*P. falciparum*) malarial drugs. Ideally, next-generation trioxolane derivatives will demonstrate curative efficacy in infected patients irrespective of the resistance status, while also offering reduced dosing frequencies and favorable pharmacokinetic properties. Moreover, such compounds should be amenable to co-formulation with a suitable partner drug, facilitating the development of robust combination therapies for global malaria control and eradication efforts (Fig. 34).

These stabilizes the endoperoxide bridge (highlighted in green and red) within the optimal pharmacological range. Considering these findings, the artefenomel-adjacent chemotype described herein exemplified by (*S*,*S*)-**151** represents a significant advancement toward the development of next-generation antimalarial combination therapies capable of delivering reliable efficacy in the context of ART-R malaria.

22. Conclusions

Over the past three decades, Griesbaum co-ozonolysis has proven to be a versatile and highly selective method for constructing 1,2,4-trioxolane scaffolds with significant biomedical relevance. Its mild conditions, broad substrate scope, and predictable diastereoselectivity have enabled applications, ranging from antimalarial and anticancer agents to diagnostic probes. Recent advances, including continuous flow ozonolysis, stabilization strategies, and rational substituent design have further enhanced its utility and scalability.

Despite these achievements, challenges remain in expanding the substrate diversity, improving the regio and stereo control

in complex systems, and deepening our mechanistic understanding. Further work in these areas is expected to unlock new opportunities in drug discovery and chemical biology, solidifying Griesbaum co-ozonolysis as a cornerstone transformation in modern synthetic chemistry.

23. Biography of Karl Griesbaum

Karl Griesbaum (1932–2019) was a German organic chemist and professor, born in Ettenheimmünster. He studied chemistry at the University of Karlsruhe and earned his PhD in 1960 under Rudolf Criegee, focusing on the mechanism of olefin ozonolysis. After a postdoctoral stint at Ohio State University (1960–1961), he worked as an industrial chemist at Esso Research (1961–1968) and then completed his habilitation in organic chemistry at Karlsruhe in 1968. He was appointed to the newly created Chair of Petrochemistry and Organic Technology at the University of Karlsruhe in 1972. Griesbaum's research spanned acetylenic chemistry, oxidation reactions, and petrochemical intermediates, with a notable focus on ozonolysis. He is best remembered for Griesbaum co-ozonolysis, first reported in 1995 as a selective method for synthesizing tetrasubstituted 1,2,4-trioxolanes *via O*-methyl ketoximes and carbonyl compounds in the presence of ozone.

Consent for publication

All the authors have given consent for the publication of the manuscript.

Author contributions

Muhammad Zain-Ul Abideen: literature survey, compilation, writing, structure drawing, Aamer Saeed: conceptualization, supervision, writing – review & editing final version; Mian Bilal Haider: editing, compilation, writing the final version, Ghulam Shabir: review and editing; Hesham R. El-Seedi: review & editing.

Conflicts of interest

The authors declare that they have no known competing financial interests or personal relationships that could have appeared to influence the work reported in this paper.

Data availability

The datasets generated and/or analyzed during the current study are available from the corresponding author upon reasonable request.

References

1 P. R. Story, R. K. Murray and H. Youssefyen, *Liebigs Ann.*, 1998, **90**(9), 2194–2195.
2 P. S. Bailey, *Ozonation in Organic Chemistry*, Academic Press, New York, 1982, vol. II, p. 55.
3 (*a*) K. Griesbaum, B. Övez and T. S. Huh, *Liebigs Ann.*, 1995, 1571–1574; (*b*) K. Griesbaum, P. Krieger-Beck and J. Beck, *Chem. Ber.*, 1991, **124**, 391–396.
4 Y. Tang, Y. Dong, J. M. Karle, C. A. DiTusa and J. L. Vennerstrom, *J. Org. Chem.*, 2004, **69**(19), 6470–6473.
5 K. Griesbaum, X. Liu, A. Kassiaris and M. Scherer, *Liebigs Ann.*, 1997, (7), 1381–1390.
6 (*a*) K. Griesbaum, X. Liu and H. Henke, *J. Org. Chem.*, 1998, **63**(4), 1086–1089; (*b*) K. J. McCullough and M. Nojima, Peroxides from Ozonization, in *Organic Peroxides*, ed. W. Ando, Wiley, Chichester, 1992, pp. 661–728.
7 K. Griesbaum, *Trends Org. Chem.*, 1997, **6**, 145.
8 K. J. McCullough and M. Nojima, Peroxides from Ozonization, in *Organic Peroxides*, ed. W. Ando, Wiley, Chichester, 1992, pp. 661–728.
9 Y. S. Hon and S. L. Yan, *Tetrahedron Lett.*, 1993, **34**, 6591–6594.
10 Y. S. Hon and J.-L. Yan, *Tetrahedron*, 1997, **53**(14), 5217–5232.
11 Y. S. Hon and J.-L. Yan, *Tetrahedron Lett.*, 1994, **35**(11), 1743–1746.
12 Y. Dong, K. Griesbaum and K. J. Mc Cullough, *J. Chem. Soc.*, 1997, 1601–1604.
13 K. Griesbaum, Y. Dong and J. McCullough, *J. Org. Chem.*, 1997, **62**(18), 6129–6136.
14 K. Griesbaum and K. Schlindwein, *J. Org. Chem.*, 1995, **60**(24), 8062–8066.
15 Y. Tang, Y. Dong, J. M. Karle, C. A. DiTusa and J. L. Vennerstrom, *J. Org. Chem.*, 2004, **69**(19), 6470–6473.
16 W. Adam, H. J. Eggelte and A. Rodriguez, *Synthesis*, 1979, **5**, 383–384.
17 J. L. Vennerstrom, Y. Dong and S. A. Charman, *Acc. Chem. Res.*, 2010, **43**(1), 145–154.
18 (*a*) K. Griesbaum, B. Övez and T. S. Huh, *Liebigs Ann.*, 1995, 1571–1574; (*b*) K. Griesbaum, P. Krieger-Beck and J. Beck, *Chem. Ber.*, 1991, **124**, 391–396; (*c*) W. H. Bunnelle, *Chem. Rev.*, 1991, **91**, 335–362.
19 M. C. Kimber and D. S. Lee, *Nat. Prod. Rep.*, 2024, **41**(5), 813–833.
20 B. W. Gung, *Chem. Rev.*, 1999, **99**(5), 1377–1386.
21 J. A. Vroman, M. Alvim-Gaston and M. A. Avery, *Curr. Pharm. Des.*, 1999, **5**(2), 101–138.
22 G. Bez, B. Kalita, P. Sarmah, N. C. Barua and D. K. Dutta, *Curr. Org. Chem.*, 2003, **7**(12), 1231–1255.
23 W. H. Bunnelle, L. A. Meyer and E. O. Schlemper, *J. Am. Chem. Soc.*, 1989, **111**(19), 7612–7613.
24 Y. Tang, Y. Dong, S. Wittlin, S. A. Charman, J. Chollet, F. C. Chiu and J. L. Vennerstrom, *Bioorg. Med. Chem. Lett.*, 2007, **17**(5), 1260–1265.
25 O. B. Kazakova, E. Y. Yamansarov, O. S. Kukovinets, N. I. Medvedeva, D. V. Kazakov, O. K. Kornilov and K. Y. Suponitskii, *Chem. Nat. Compd.*, 2011, **47**, 738–740.
26 G. J. Ten Brink, I. W. C. E. Arends and R. A. Sheldon, *Chem. Rev.*, 2004, **104**(9), 4105.
27 G. G. Holmes and J. M. Smith, *Org. Biomol. Chem.*, 2018, **16**(22), 4530–4542.

28 Y. Tang, Y. Dong, J. M. Karle, C. A. DiTusa and J. L. Vennerstrom, *J. Org. Chem.*, 2004, **69**(19), 6470–6473.
29 F. W. Semmler, *Ber. Dtsch. Chem. Ges.*, 1909, **42**, 246.
30 O. B. Kazakova, D. V. Kazakov, E. Y. Yamansarov, N. Y. I. Medvedeva, G. A. Tolstikov, K. Y. Suponitsky and D. E. Arkhipov, *Tetrahedron Lett.*, 2011, **52**(9), 976–979.
31 K. Griesbaum, X. Liu and H. Henke, *J. Org. Chem.*, 1998, **63**(4), 1086–1089.
32 (*a*) Y. Dong, X. Wang, S. Kamaraj, V. J. Bulbule, F. C. Chiu, J. Chollet and J. L. Vennerstron, *J. Med. Chem.*, 2017, **60**(7), 2654–2668; (*b*) N. I. Medvedeva, O. B. Flekhter, L. A. Baltina, F. Z. Galin and G. A. Tolstikov, *Chem. Nat. Compd.*, 2004, **40**, 247–249.
33 Y. Tang, Y. Dong, J. M. Karle, C. A. DiTusa and J. L. Vennerstrom, *J. Org. Chem.*, 2004, **69**(19), 6470–6473.
34 Y. Dong, J. Chollet, H. Matile, S. A. Charman, F. C. K. Chiu, W. N. Charman, B. Scorneaux, H. Urwyler, J. Santo Tomas, C. Scheurer, C. Snyder, A. Dorn, X. Wang, J. M. Karle, Y. Tang, S. Wittlin, R. Brun and J. L. Vennerstrom, *J. Med. Chem.*, 2005, **48**(15), 4953–4961.
35 K. Griesbaum, B. Övez and T. S. Huh, *Liebigs Ann.*, 1995, 1571–1574.
36 K. Griesbaum, X. Liu, A. Kassiaris and M. Scherer, *Liebigs Ann.*, 1997, (7), 1381–1390.
37 (*a*) T. J. Fisher and P. H. Dussault, *Tetrahedron*, 2017, **73**(30), 4233–4258; (*b*) Y. Dong, X. Wang, S. Kamaraj, V. J. Bulbule, F. C. Chiu, J. Chollet and J. L. Vennerstrom, *J. Med. Chem.*, 2017, **60**(7), 2654–2668.
38 A. O. Terent'ev, D. A. Borisov, V. A. Vil and V. M. Dembitsky, *Beilstein J. Org. Chem.*, 2014, **10**(1), 34–114.
39 G. Gabriel dos Passos Gomes, I. A. Yaremenko, P. S. Radulov, R. A. Novikov, V. V. Chernyshev, A. A. Korlyukov, G. I. Nikishin, I. V. Alabugin and A. O. Terent'ev, *Angew. Chem., Int. Ed.*, 2017, **56**, 4955–4959.
40 J. L. Vennerstrom, S. Arbe-Barnes, R. Brun, S. A. Charman, F. C. Chiu, J. Chollet and W. N. Charman, *Nature*, 2004, **430**(7002), 900–904.
41 O. B. Kazakova, E. F. Khusnutdinova, G. A. Tolstikov and K. Y. Suponitsky, *Russ. J. Bioorg. Chem.*, 2010, **36**(4), 512–515.
42 J. L. Vennerstrom, S. Arbe-Barnes, R. Brun, S. A. Charman, F. C. Chiu, J. Chollet and W. N. Charman, *Nature*, 2004, **430**(7002), 900–904.
43 S. D. Fontaine, A. G. DiPasquale and A. R. Renslo, *Org. Lett.*, 2014, **16**(21), 5776–5779.
44 Y. Dong, X. Wang, S. Kamaraj, V. J. Bulbule, F. C. Chiu, J. Chollet and J. L. Vennerstrom, *J. Med. Chem.*, 2017, **60**(7), 2654–2668.
45 Y. Dong, S. Wittlin, K. Sriraghavan, J. Chollet, S. A. Charman, W. N. Charman, C. Scheurer, H. Urwyler, J. Santo Tomas, C. Snyder, D. J. Creek, J. Morizzi, M. Koltun, H. Matile, X. Wang, M. Padmanilayam, Y. Tang, A. Dorn, R. Brun and J. L. Vennerstrom, *J. Med. Chem.*, 2010, **53**(1), 481–491.
46 M. T. Klope, J. A. Tapia Cardona, J. Chen, R. L. Gonciarz, K. Cheng, P. Jaishankar and A. R. Renslo, *ACS Med. Chem. Lett.*, 2024, **15**(10), 1764–1770.
47 Y. Dong, Y. Tang, J. Chollet, H. Matile, S. Wittlin, S. A. Charman and J. L. Vennerstrom, *Bioorg. Med. Chem.*, 2006, **14**(18), 6368–6382.
48 A.-J. Lin, D. L. Klayman and W. K. Milhous, *J. Med. Chem.*, 1987, **30**(11), 2147–2150.
49 L. Zhou, A. Alker, A. Ruf, X. Wang, F. C. Chiu, J. Morizzi and J. L. Vennerstrom, *Bioorg. Med. Chem. Lett.*, 2008, **18**(5), 1555–1558.
50 (*a*) W. Adcock and N. A. Trout, *Chem. Rev.*, 1999, **99**, 1415; (*b*) B. W. Gung, *Chem. Rev.*, 1999, **99**, 1377.
51 E. Tsandi, C. G. Kokotos, S. Kousidou, V. Ragoussis and G. Kokotos, *Tetrahedron*, 2009, **65**(7), 1444–1449.
52 Y. Dong, S. Wittlin, K. Sriraghavan, J. Chollet, S. A. Charman, W. N. Charman, C. Scheurer, H. Urwyler, J. Santo Tomas, C. Snyder, D. J. Creek, J. Morizzi, M. Koltun, H. Matile, X. Wang, M. Padmanilayam, Y. Tang, A. Dorn, R. Brun and J. L. Vennerstrom, *J. Med. Chem.*, 2010, **53**(1), 481–491.
53 T. Itoh, T. Wanibe and S. Iwatsuki, *J. Polym. Sci.*, 1996, **34**(6), 963–969.
54 Y. Dong and J. L. Vennerstrom, *J. Org. Chem.*, 1998, **63**(23), 8582–8585.
55 (*a*) C. Battilocchio, I. R. Baxendale, M. Biava, M. O. Kitching and S. V. Ley, *Org. Process Res. Dev.*, 2012, **16**(5), 798–810; (*b*) M. O'Brien, I. R. Baxendale and S. V. Ley, *Org. Lett.*, 2010, **12**(7), 1596–1598.
56 T. Ouchi, C. Battilocchio, J. M. Hawkins and S. V. Ley, *Org. Process Res. Dev.*, 2014, **18**(11), 1560–1566.
57 (*a*) K. Borstnik, I. Paik, T. Shapiro and G. H. Posner, *Int. J. Parasitol.*, 2002, **32**(13), 1661; (*b*) S. H. Lau, A. Galván, R. R. Merchant, C. Battilocchio, J. A. Souto, M. B. Berry and S. V. Ley, *Org. Lett.*, 2015, **17**(13), 3218–3221.
58 S. H. Lau, A. Galván, R. R. Merchant, C. Battilocchio, J. A. Souto, M. B. Berry and S. V. Ley, *Org. Lett.*, 2015, **17**(13), 3218–3221.
59 S. D. Fontaine, B. Spangler, J. Gut, E. M. Lauterwasser, P. J. Rosenthal and A. R. Renslo, *ChemMedChem*, 2015, **10**(1), 47–51.
60 A. T. Aron, M. O. Loehr, J. Bogena and C. J. Chang, *J. Am. Chem. Soc.*, 2016, **138**(43), 14338–14346.
61 S. V. Torti and F. M. Torti, *Nat. Rev. Cancer*, 2013, **13**(5), 342–355.
62 S. V. Torti and M. F. Torti, *Cancer Res.*, 2011, **71**(95), 1511–1514.
63 B. Spangler, C. W. Morgan, S. D. Fontaine, M. N. Vander Wal, C. J. Chang, J. A. Wells and A. R. Renslo, *Nat. Chem. Biol.*, 2016, **12**(9), 680–685.
64 A. R. Bogdan, M. Miyazawa, K. Hashimoto and Y. Tsuji, *Trends Biochem. Sci.*, 2016, **41**(3), 274–286.
65 S. J. Dixon and B. R. Stockwell, *Nat. Chem. Biol.*, 2014, 9–17.
66 C. Zhang and F. Zhang, *Protein Cell*, 2015, **6**(2), 88–100.
67 W. S. Yang and B. R. Stockwell, *Chem. Biol.*, 2008, **15**(3), 234–245.
68 J. Chen, R. L. Gonciarz and A. R. Renslo, *RSC Adv.*, 2021, **11**(54), 34338–34342.
69 J. Matsumoto, Y. Dong and J. L. Vennerstrom, *Org. Biomol. Chem.*, 2018, **16**(12), 2187–2195.

70 S. A. Charman, S. Arbe-Barnes, I. C. Bathurst, R. Brun, M. Campbell, W. N. Charman and J. L. Vennerstrom, *Proc. Natl. Acad. Sci. U. S. A.*, 2011, **108**(11), 4400–4405.

71 (*a*) A. T. Aron, A. G. Reeves and C. J. Chang, *Curr. Opin. Chem. Biol.*, 2018, **43**, 113; (*b*) C. J. Chang, *Nat. Chem. Biol.*, 2015, **11**(10), 744; (*c*) K. J. Bruemmer, S. W. M. Crossley and C. J. Chang, *Angew. Chem., Int. Ed.*, 2020, **59**(33), 13734; (*d*) T. Hirayama, *Free Radical Biol. Med.*, 2019, **133**, 38–45.

72 B. Spangler, C. W. Morgan, S. D. Fontaine, M. N. VanderWal, C. J. Chang, J. A. Wells and A. R. Renslo, *Nat. Chem. Biol.*, 2016, **12**(9), 680–685.

73 A. T. Aron, M. C. Heffern, Z. R. Lonergan, M. N. Vander Wal, B. R. Blank, B. Spangler, Y. Zhang, H. M. Park, A. Stahl, A. R. Renslo, E. P. Skaar and C. J. Chang, *Proc. Natl. Acad. Sci. U. S. A.*, 2017, **114**(48), 12669–12674.

74 S. Xu, H. W. Liu, L. Chen, J. Yuan, Y. Liu, L. Teng, S. Y. Huan, L. Yuan, X. B. Zhang and W. Tan, *J. Am. Chem. Soc.*, 2020, **142**(5), 2129–2133.

75 N. Zhao, Y. Huang, Y. H. Wang, R. K. Muir, Y. C. Chen, N. Hooshdaran, J. Wei, P. Viswanath, Y. Seo, D. Ruggero, A. R. Renslo and M. J. Evans, *J. Nucl. Med.*, 2021, **62**(7), 949–955.

76 R. K. Muir, N. Zhao, J. Wei, Y. H. Wang, A. Moroz, Y. Huang, Y. C. Chen, R. Sriram, J. Kurhanewicz, D. Ruggero, A. R. Renslo and M. J. Evans, *ACS Cent. Sci.*, 2019, **5**(4), 727–736.

77 Y. C. Chen, J. A. Oses-Prieto, L. E. Pope, A. L. Burlingame, S. J. Dixon and A. R. Renslo, *J. Am. Chem. Soc.*, 2020, **142**(45), 19085–19093.

78 S. D. Fontaine, A. G. DiPasquale and A. R. Renslo, *Org. Lett.*, 2014, **16**(21), 5776–5779.

79 J. Wu, X. Wang, F. C. K. Chiu, C. Haberli, D. M. Shackleford, E. Ryan, S. Kamaraj, V. J. Bulbule, A. I. Wallick, Y. Dong, K. L. White, P. H. Davis, S. A. Charman, J. Keiser and J. L. Vennerstrom, *J. Med. Chem.*, 2020, **63**(7), 3723–3736.

80 E. Y. Yamansarov, O. B. Kazakova, N. I. Medvedeva, D. V. Kazakov, O. S. Kukovinets and G. A. Tolstikov, *Russ. J. Org. Chem.*, 2014, **50**(7), 1043–1047.

81 O. B. Kazakova, E. F. Khusnutdinova, A. V. Petrova, E. Y. Yamansarov, A. N. Lobov, A. A. Fedorova and K. Y. Suponitsky, *J. Nat. Prod.*, 2019, **82**(9), 2550–2558.

82 B. R. Blank, R. L. Gonciarz, P. Talukder, J. Gut, J. Legac, P. J. Rosenthal and A. R. Renslo, *ACS Infect. Dis.*, 2020, **6**(7), 1827–1835.

83 E. M. W. Lauterwasser, S. D. Fontaine, H. Li, J. Gut, K. Katneni, S. A. Charman, P. J. Rosenthal, M. Bogyo and A. R. Renslo, *ACS Med. Chem. Lett.*, 2015, **6**(11), 1145–1149.

84 P. S. Sijwali and P. J. Rosenthal, *Proc. Natl. Acad. Sci. U. S. A.*, 2004, **101**(13), 4384–4389.

85 S. D. Fontaine, B. Spangler, J. Gut, E. M. Lauterwasser, P. J. Rosenthal and A. R. Renslo, *ChemMedChem*, 2015, **10**(1), 47–51.

86 (*a*) B. R. Blank, P. Talukder, R. K. Muir, E. R. Green, E. P. Skaar and A. R. Renslo, *ACS Infect. Dis.*, 2019, **5**(8), 1366–1375; (*b*) B. R. Blank, J. Gut, P. J. Rosenthal and A. R. Renslo, *ACS Med. Chem. Lett.*, 2023, **14**(4), 493–498.

87 S. S. Mahajan, E. Deu, E. M. W. Lauterwasser, M. J. Leyva, J. A. Ellman, M. Bogyo and A. R. Renslo, *ChemMedChem*, 2011, **6**(3), 415–419.

88 C. M. Woodley, G. L. Nixon, N. Basilico, S. Parapini, W. D. Hong, S. A. Ward, G. A. Biagini, S. C. Leung, D. Taramelli, K. Onuma, T. Hasebe and P. M. O'Neill, *ACS Med. Chem. Lett.*, 2021, **12**(7), 1077–1085.

89 B. R. Blank, J. Gut, P. J. Rosenthal and A. R. Renslo, *ACS Med. Chem. Lett.*, 2023, **14**(4), 493–498.

90 (*a*) M. T. Klope, J. A. Tapia Cardona, J. Chen, R. L. Gonciarz, K. Cheng, P. Jaishankar and A. R. Renslo, *ACS Med. Chem. Lett.*, 2024, **15**(10), 1764–1770; (*b*) M. T. Klope, P. Talukder, B. R. Blank, S. Chelebieva, J. Chen, S. D. Fontaine and A. R. Renslo, *bioRxiv*, 2025, preprint, DOI: **10.1101/2025.01.02.631109**.